iScience

CellPress

Article

Spermidine Suppresses Inflammatory DC Function by Activating the FOXO3 Pathway and Counteracts Autoimmunity

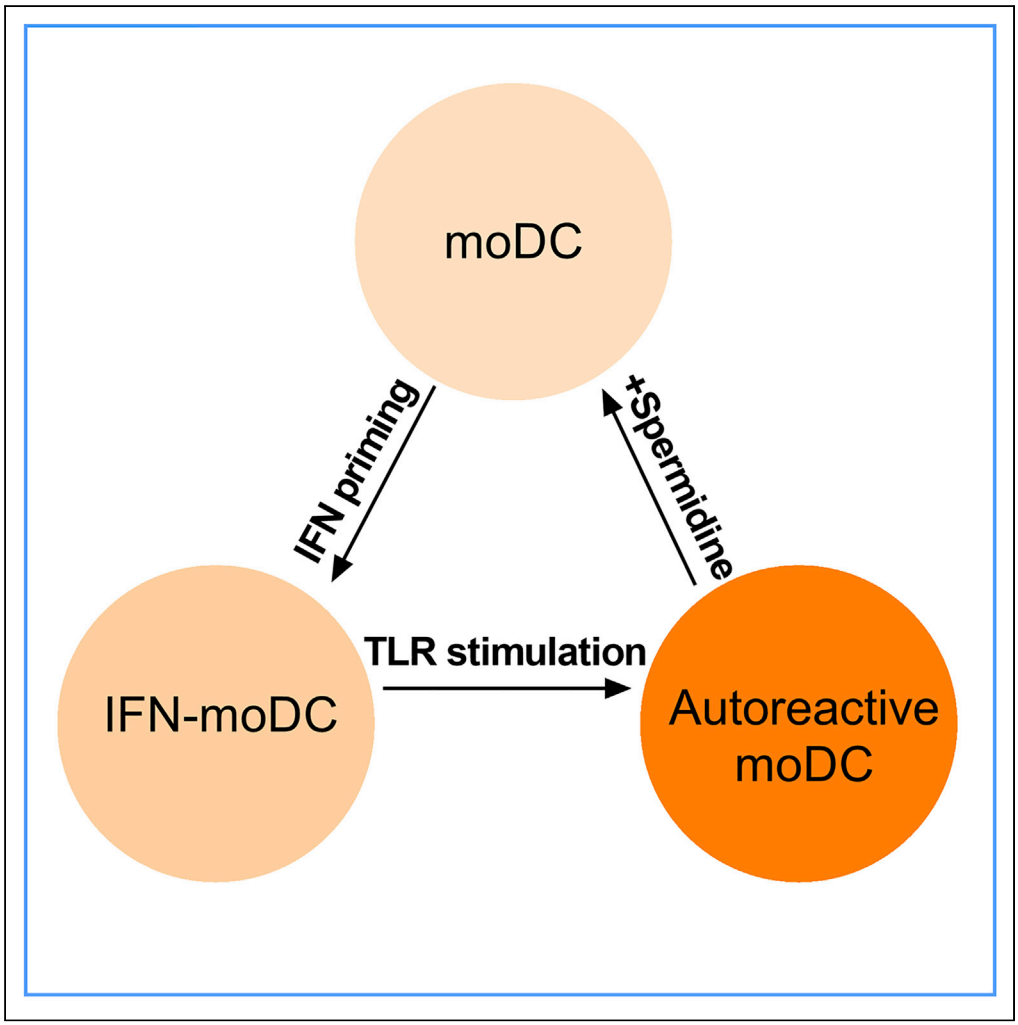

Guanhua Li, Huihua Ding, Xiang Yu, ..., Qiang Guo, Haibo Zhou, Nan Shen

hbzhou1984@gmail.com (H.Z.)
nanshensibs@gmail.com (N.S.)

HIGHLIGHTS

Spermidine decreases in IFN-primed and TLR7 ligand-stimulated dendritic cells

Spermidine suppresses the activation of inflammatory dendritic cells

FOXO3 pathway mediates the function of spermidine

Spermidine supplement alleviated the development of psoriasis-like symptom

Li et al., iScience *23*, 100807
January 24, 2020
https://doi.org/10.1016/j.isci.2019.100807

iScience

CellPress

Article

Spermidine Suppresses Inflammatory DC Function by Activating the FOXO3 Pathway and Counteracts Autoimmunity

Guanhua Li,[1] Huihua Ding,[1] Xiang Yu,[1] Yao Meng,[1] Jun Li,[1] Qiang Guo,[1] Haibo Zhou,[1,2,*] and Nan Shen[1,2,3,4,5,6,*]

SUMMARY

Dendritic cells (DCs) function is intimately linked to microenvironment and metabolism. Type I interferons (IFNs) condition dendritic cells to respond to weak self-signals, leading to autoimmunity. However, the metabolic adaption in the process is unclear. Here, we identified spermidine as a critical metabolite impacting the metabolic fitness of DC. First, dynamic metabolome screening indicated that spermidine decreased during IFN priming and following TLR7 ligand stimulation, accompanied by metabolic change from oxidative phosphorylation to glycolysis. Second, spermidine supplement restrained the glycolysis and prevented the overactivation of IFN-α primed DC both *in vivo* and *in vitro*. Third, mechanism study uncovered that the activity of FOXO3 adapted to the metabolic change, mediating the anti-inflammatory effect of spermidine. More importantly, addition of spermidine *in vivo* greatly alleviated the development of psoriasis-like symptom in mice. Thus, our studies revealed metabolic changes boosting DC responses and identified spermidine as a potential therapeutic agent for autoimmune diseases.

INTRODUCTION

Dendritic cells (DCs) are a distinct lineage of mononuclear phagocyte, specialized in antigen presentation to T cells and the control of immunity. Multiple subtypes of DC that have distinct functions and molecular characteristics have been identified (Durai and Murphy, 2016; Malissen et al., 2014; Merad et al., 2013; Shortman and Naik, 2007; Worbs et al., 2017). There are three major subsets of DCs: plasmacytoid DCs (pDCs), conventional DCs (cDCs), and monocyte-derived DCs (moDCs). PDCs are a distinct lineage of DCs that are more specialized for cytokine production, particularly type I interferon (IFN) production, rather than antigen presentation. CDCs within non-lymphoid tissue are composed of two major subpopulations, which are distinguished by the expression of CD103 or CD11b, migrating to lymphoid node and maintaining homeostasis in the steady state (Merad et al., 2013; Shortman and Naik, 2007). In the inflammatory state, monocytes can infiltrate lesion sites and develop into inflammatory myeloid DCs (mDCs) producing tumor necrosis factor (TNF)-α, interleukin (IL)-12, and IL-23 with the activation of both T helper (Th)1 and Th17 cells (Malissen et al., 2014; Worbs et al., 2017). It is known from a wide range of studies that type I IFNs alone or in combination with other cytokines and growth factors such as granulocyte/monocyte colony-stimulating factor (GM-CSF) promote the differentiation and activation of DCs derived from monocytes (Blanco et al., 2001; Farkas and Kemeny, 2012; Postat et al., 2018; Rodriguez-Pla et al., 2014; Santini et al., 2011). IFN-α effectively abrogates Toll-like receptor (TLR)-induced cross-tolerance by priming chromatin to enable moDC to produce robust transcriptional responses to weak signals, leading to the immune response out of control. Furthermore, IFN-α primed moDCs (IFN-DCs) upregulate TLR7 expression and response to self-RNA, which is absent in GM-CSF-induced moDCs (Mohty et al., 2003). Therefore, IFN-DCs are considered to be critical for the pathology of autoimmune disorders such as systemic lupus erythematosus (SLE) and psoriasis (Ganguly, 2018).

It is becoming increasingly clear that different stages of DC activation coincide with different types of cellular metabolism to satisfy the bioenergetic and biosynthetic needs of these cells (Everts and Pearce, 2014; O'Neill and Pearce, 2016; Pearce and Everts, 2015; Postat et al., 2018; Wu et al., 2016). Under non-inflammatory conditions, catabolic metabolism in DCs centered on mitochondrial oxidative phosphorylation (OXPHOS) is associated with cellular longevity and quiescence. Upon TLR agonists stimulation, DCs undergo a robust metabolic switch characterized by an increase in glycolysis and a progressive loss of OXPHOS signaling (Everts and Pearce, 2014; O'Neill and Pearce, 2016; Pearce and Everts, 2015). Pathways regulating these metabolic states have been uncovered. The conserved kinase mammalian/mechanistic

[1]Shanghai Institute of Rheumatology, Renji Hospital, Shanghai Jiao Tong University School of Medicine (SJTUSM), 145 Shan Dong Middle Road, Shanghai 200001, China

[2]Shenzhen Futian Hospital for Rheumatic Diseases, Shenzhen 518040, China

[3]Center for Autoimmune Genomics and Etiology (CAGE), Cincinnati Children's Hospital Medical Center, Cincinnati, OH, USA

[4]Department of Pediatrics, University of Cincinnati College of Medicine, Cincinnati, OH, USA

[5]State Key Laboratory of Oncogenes and Related Genes, Shanghai Cancer Institute, Renji Hospital, Shanghai Jiao Tong University School of Medicine (SJTUSM), Shanghai 200032, China

[6]Lead Contact

*Correspondence: hbzhou1984@gmail.com (H.Z.), nanshensibs@gmail.com (N.S.)

https://doi.org/10.1016/j.isci.2019.100807

target of rapamycin (mTOR) and its upstream activators phosphoinositide 3-kinase (PI3K)-Akt have been identified as central regulators promoting glycolysis and anabolic metabolism, whereas AMP Kinase (AMPK) is found antagonizing biosynthetic pathways and promoting mitochondrial biogenesis to increase mitochondrial OXPHOS (Everts and Pearce, 2014; O'Neill and Pearce, 2016; Pearce and Everts, 2015). Balance between mTOR and AMPK determines the TLR-induced glucose consumption, mitochondrial OXPHOS, and thereby the immunogenic properties of DC (Everts and Pearce, 2014; O'Neill and Pearce, 2016; Pearce and Everts, 2015).

Metabolic reprograming of DCs is particularly crucial in autoimmune responses because nutrients often change dramatically in autoimmune patients (Everts and Pearce, 2014). In addition to the proven epigenetic regulation (Park et al., 2017), cytokines, such as type I IFNs, in the self-reactive environment may also affect the metabolic state of DC, thus making it more easily activated. Emerging studies have revealed molecules and pathways involved in the aberrant activation of DC upon IFN priming. However, few studies clarify the metabolic changes in the process.

Here, we screened the change of amino acids and their derivates in DC during IFN-priming and TLR7-activating stages. In particular, the levels of spermidine decreased continuously in both processes. Meanwhile, IFN-α priming and TLR7 ligand stimulation skewed the metabolism of DC from mitochondrial OXPHOS toward glycolysis. Meanwhile, the AMPK pathway was inhibited and the mTORC1 pathway was activated. Addition of spermidine reversed the process and prevented DC activation. Mechanism study further identified that the phosphorylation sites of FOXO3 changed with the metabolic status and mediated the anti-inflammatory effect of spermidine at the transcriptional factor level. Genetic deletion of *foxo3a* weakened the function of spermidine. More importantly, supplement of spermidine alleviated the psoriasis-like symptoms and systematic inflammation in an imiquimod (IMQ)-induced psoriasis-like mouse model. Therefore, our results highlight spermidine as a key metabolite in DCs, necessary to maintain normal immune responses and treat autoimmune diseases.

RESULTS

Metabolomic Changes during IFN Priming and following TLR Activation of DCs

DCs in this paper were generated by GM-CSF cultured monocytes isolated from bone marrow, so we used "moDC" instead of the commonly used "BMDC." Previous works have reported that type I IFN induced the differentiation of DC and promoted the inflammatory function of DC in autoimmune diseases (Everts and Pearce, 2014; Wu et al., 2016). We also confirmed that IFN-DC produced large amounts of TNF-α and IL-6 after TLR7 ligand stimulation, whereas moDC was unresponsive (Figure 1A). Correspondingly, the expression of TLR7 mRNA was induced, significantly (Figure 1A).

To investigate the metabolic adaptations underlying both IFN priming and DC activation, we analyzed the intracellular amino acids and their derivates in GM-CSF-induced moDCs by mass spectrometry. MoDCs were cultured with IFN-α for 24 h first and then stimulated with TLR7 ligand R837 for different time points (Figure S1). After cell lysis, proteins were digested and analyzed by ultra-performance liquid chromatography coupled to tandem mass spectrometry (UPLC-MS/MS). Results showed that most amino acids decreased in the stage of IFN priming, whereas L-citrulline, aspartic acid, and taurine showed an increasing trend (Figure 1B). Similarly, most amino acids decreased in the TLR ligand-stimulating stage. In contrast, L-arginine and L-glutamine increased first and then decreased, whereas L-citrulline, taurine, and methionine sulfoxide dropped rapidly in 4 h and then increased (Figure 1C).

Interestingly, the derivates of L-arginine exhibited different changes in the two processes. L-arginine metabolic pathway consists of the L-arginine-nitric oxide (NO) pathway and polyamine catabolism pathway (Babicova et al., 2011; Locke et al., 2016; Mondanelli et al., 2017). As the major components of polyamine catabolism (Locke et al., 2016), both spermidine and spermine decreased during IFN priming and following TLR7 ligand stimulation (Figures 1B and 1C). On the contrary, L-citrulline, major metabolic intermediates of L-arginine-NO pathway (Locke et al., 2016), increased from 4 to 16 h of TLR7 ligand stimulation. L-arginine showed no obvious change in the IFN-priming stage but increased significantly in the IFN-DC maturation stage (Figures 1B and 1C). It indicated that L-arginine was mainly directed to the L-arginine-NO pathway at the expense of polyamine synthesis. The changes in metabolic pathways may be adapted to the changes in DC function. Meanwhile, we detected the expression of enzymes (Geiger et al., 2016; Locke et al., 2016). IFN-α priming led to reduction of enzymes controlling polyamine synthesis, including arginase 1 (*Arg1*),

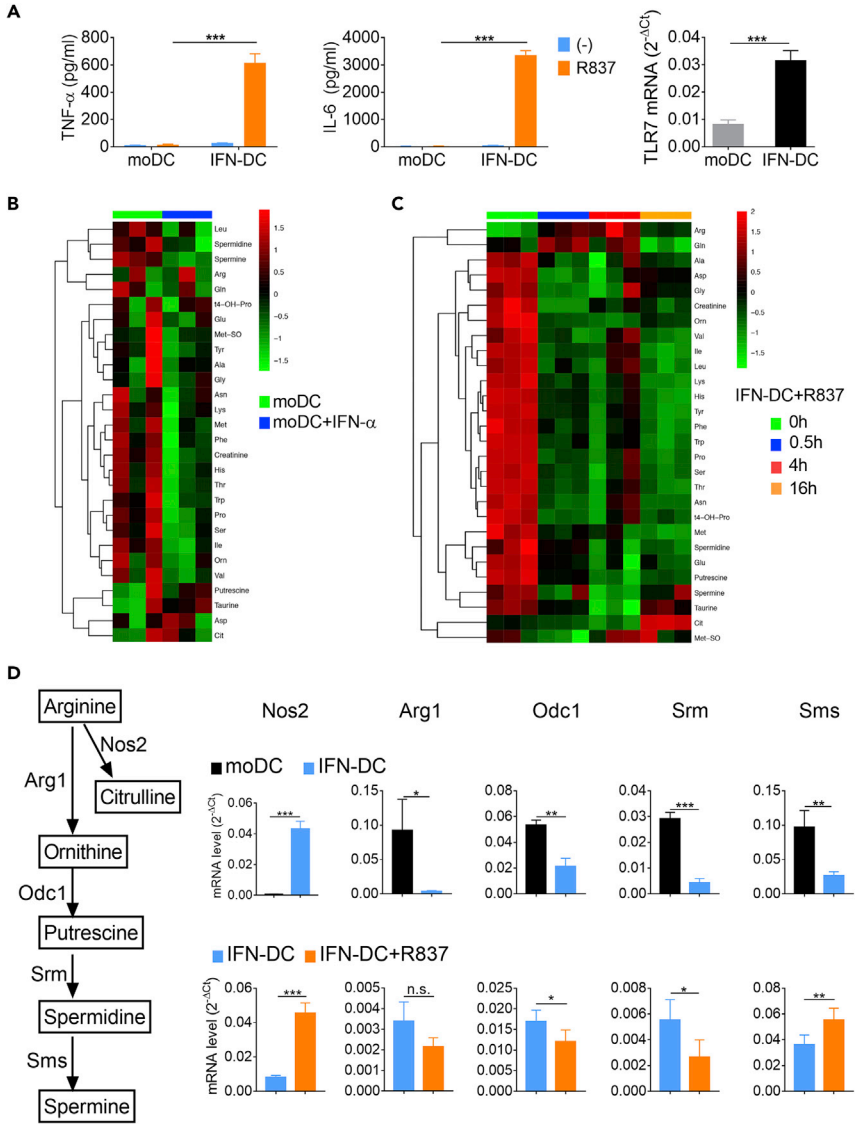

Figure 1. Metabolomic Changes during IFN Priming and Following TLR Activation of DCs

BM monocytes were cultured with GM-CSF and IL-4 for 7 days. MoDCs were sorted and treated with 2,000 U/mL IFN-α for 24 h (IFN priming).

(A) The moDCs and IFN-α-primed moDCs (IFN-DCs) were stimulated with 10 μg/mL R837 for 24 h. The protein levels of TNF-α and IL-6 secreted from moDCs and IFN-DCs were detected. And the mRNA levels of *TLR7* in moDCs and IFN-DCs were detected. Data are representative of three independent experiments. Error bars represent SEM. P values were determined by two-tailed unpaired t test.

(B and C) MoDCs were primed with IFN-α for 24 h. IFN-DCs were stimulated with or without 10 μg/mL R837 for 0.5, 4, or 16 h (IFN-DCs maturation). Then, moDCs and IFN-DCs were collected and the lysate was analyzed by UPLC-MS/MS. (B) Heatmap of the amino acids and their derivates changes in moDCs (n = 3). (C) Heatmap of the amino acids and their derivates changes during IFN-DC maturation (n = 3). Colors represent the levels of the metabolites from low (green) to high (red).

(D) Changes of metabolic enzymes during IFN-priming stage and IFN-DC maturation stage. The expression of mRNAs was normalized to *β-actin* mRNA by calculating $2^{-\Delta Ct}$. Data are representative of three independent experiments. Error bars represent SEM. P values were determined by two-tailed unpaired *t* test *p < 0.05, **p < 0.01, ***p < 0.001. n.s., not significant.

ornithine decarboxylase 1 (*Odc1*), spermidine synthase (*Srm*), and spermine synthase (*Sms*). In contrast, *Nos2*, which catalyzes the production of NO from L-arginine, was induced by IFN-α, significantly. During TLR7 ligand stimulation, *Srm* and *Odc1* decreased, whereas *Nos2* and *Sms* increased (Figure 1D), leading

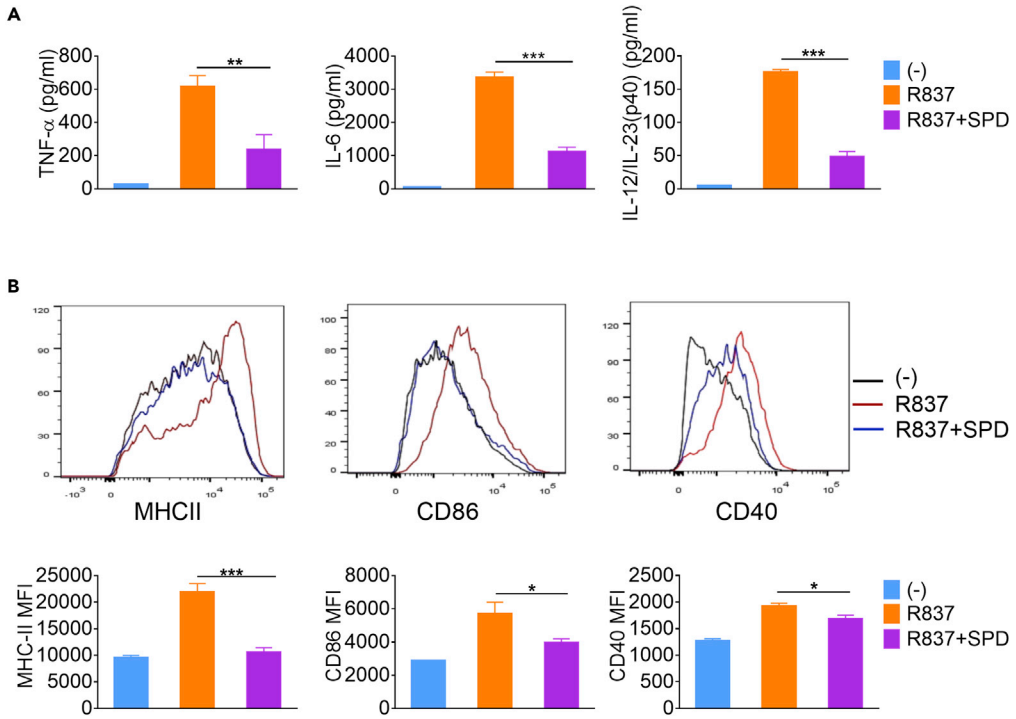

Figure 2. Spermidine Inhibits IFN-DC Activation

BM monocytes were cultured with GM-CSF and IL-4 for 7 days. MoDCs were sorted and treated with 2,000 U/mL IFN-α for 24 h, and then the IFN-DCs were stimulated with 10 μg/mL R837 in the presence or absence of spermidine (SPD) for 24 h.

(A) The protein levels of TNF-α, IL-6, and IL-12/23 p40 (n = 3).

(B) Flow cytometry analysis of MHCII, CD80, and CD40 (n = 3). Data are representative of three independent experiments. Error bars represent SEM. P values were determined by two-tailed unpaired t test *p < 0.05, **p < 0.01, ***p < 0.001.

to the further reduction of spermidine and increase of L-citrulline. The changes in the mRNA levels of these metabolic enzymes were consistent with changes in metabolites. Therefore, L-arginine and its derivatives might be more critical for the pro-inflammatory function of IFN-DC.

Spermidine Inhibits IFN-DC Activation

It is clear that iNOS and the production of NO could enhance the immunologic function of DC by influencing the metabolism of pathogenic microorganisms (Pearce and Everts, 2015). However, the function of polyamine on DC, especially for IFN-DC, is still unclear. Spermidine was chosen for further study as it decreased most significantly, compared with other polyamines. To investigate the effect of spermidine on IFN-DC activation, moDCs were cultured with IFN-α for 24 h and then stimulated with R837, together with spermidine or not, for another 24 h. The survival of IFN-DC was not affected at the indicated concentration of spermidine (Figure S2A). Compared with control, addition of spermidine led to the reduction of 61.5%, 66.8%, and 72.4% in the expression of TNF-α, IL-6, and IL-12/23 p40, respectively (Figure 2A). In line with this, the expression of major histocompatibility complex (MHC) II and co-stimulatory molecules CD86 and CD40 was also suppressed by spermidine, showing that their mean fluorescence intensities decreased by 51.7%, 30.4%, and 12.3%, respectively (Figure 2B). On the contrary, blocking the synthesis of spermidine by using difluoromethylornithine (DFMO) augmented the activation of moDCs (Figure S2B). Moreover, spermidine exerted inhibitory effects not only in the TLR-stimulating stage, but also in the IFN-priming stage. Addition of spermidine during IFN priming inhibited the expression of TLR7, TNF-α, and IL-6 (Figures S2C and S2D). Therefore, spermidine is a negative regulator of IFN-DC activation.

Besides, we also detected the function of spermidine during other TLR ligands stimulation. Interestingly, it inhibited the CpG activation of moDC but had little effects on LPS activation (Figure S2E). Thus, its function varied with stimulus.

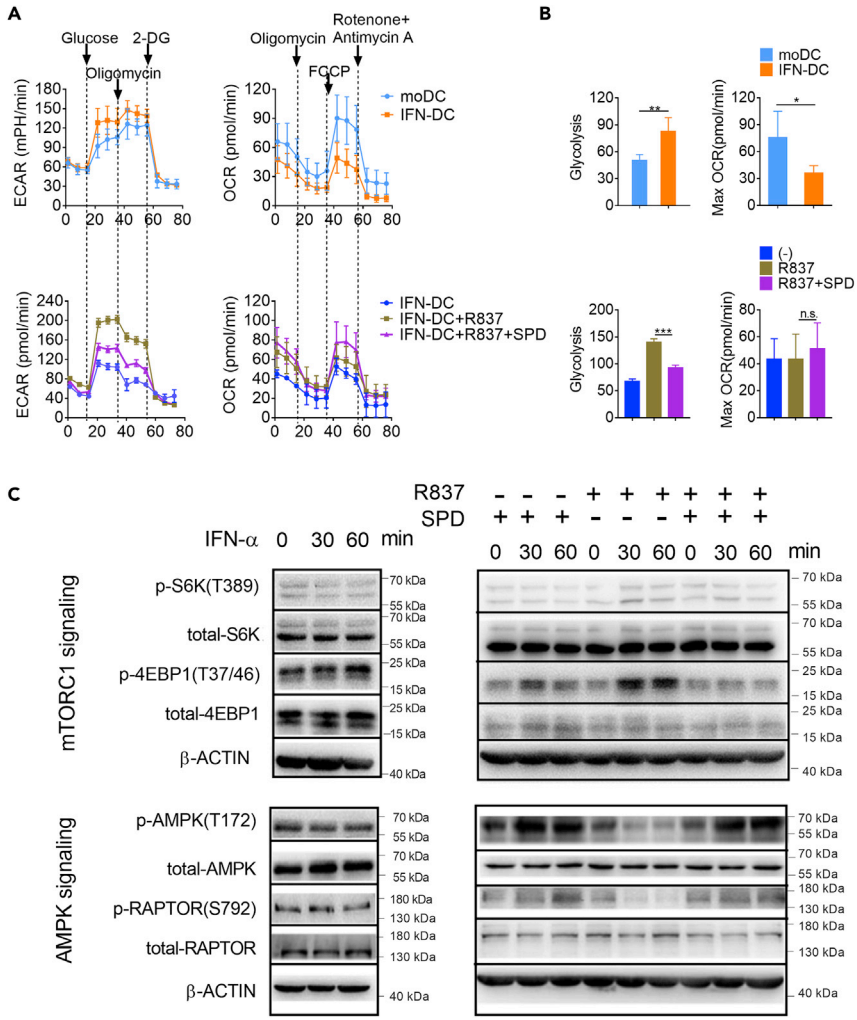

Figure 3. Spermidine Enforces Metabolic Quiescence in IFN-DCs

BM monocytes were cultured with GM-CSF and IL-4 for 7 days. MoDCs were sorted and treated with 2,000 U/mL IFN-α for 24 h, and then the IFN-DCs were stimulated with 10 μg/mL R837 in the presence or absence of spermidine (SPD) for 24 h.
(A) The extracellular acidification rate (ECAR) (left) and oxygen consumption rate (OCR) (right) were detected (n = 4).
(B) Statistics of glycolysis and maximum OCR are shown (n = 4). Data are shown as mean ± SEM. P values were determined by two-tailed unpaired t test *p < 0.05, **p < 0.01, ***p < 0.001. n.s., not significant.
(C) MoDCs or IFN-DCs were treated with IFN-α, R837, or R837 and spermidine for the indicated times, respectively. The levels of protein were analyzed by immunoblot. β-ACTIN was used as the internal loading control. Data are representative of three independent experiments.

Spermidine Enforces Metabolic Quiescence in IFN-DCs

Functional changes are often accompanied by changes in intracellular metabolism. We next assessed the consequences of increasing spermidine availability on IFN-DC metabolism. MoDCs were cultured with IFN-α for 24 h and then stimulated with R837, together with spermidine or not, for another 24 h. Then, we measured the extracellular acidification rate (ECAR, an indicator of glycolysis) and oxygen consumption rate (OCR, an indicator of OXPHOS) (Figure 3A). Compared with moDCs, IFN-DCs exhibited increased glycolysis and diminished OXPHOS. TLR7 ligand stimulation further enhanced glycolysis. On the contrary, spermidine supplement restrained the glycolytic flux obviously (Figures 3A and 3B). Oxygen consumption also increased slightly upon spermidine treatment, although there was no statistically significant difference.

To study the mechanisms causing the metabolic status changes in moDCs and IFN-DCs, we analyzed critical pathways regulating glycolysis and mitochondrial OXPHOS. In the IFN-priming stage, the

phosphorylation levels of AMPK and RAPTOR decreased, whereas the phosphorylation of eukaryotic initiation factor 4E (eIF4E)-binding protein 1 (4EBP1) increased, corresponding to the diminished OXPHOS and elevated glycolysis (Figures 3A–3C). In the TLR7 ligand stimulating stage, the phosphorylation levels of AMPK and RAPTOR continued to decline, whereas the phosphorylation of 70 ribosomal protein S6 kinase (S6K) and 4EBP1, two signaling transducers downstream mTORC1, were induced (Figure 3C). On the contrary, addition of spermidine promoted the activation of AMPK and RAPTOR regardless of the existence of TLR7 ligand stimulation. Meanwhile, spermidine hampered the activation of S6K and 4EBP1 in the presence of R837. Therefore, spermidine activates the AMPK pathway and inhibits the mTORC1 pathway in IFN-DCs.

FOXO3 Mediates the Anti-inflammatory Effect of Spermidine

To clarify the critical transcription factor mediating the anti-inflammatory effect of spermidine, IFN-DCs were cultured with R837, together with or without spermidine, for 18 h. RNA sequencing analysis showed that genes enriched in autoimmune diseases and inflammatory responses were suppressed by spermidine (Schwartz et al., 2016), supporting the anti-inflammatory roles of spermidine in IFN-DCs (Figure S3). Notably, genes in the JAK/STAT pathway and the NF-κB pathway were inhibited by spermidine. As a result, the pro-inflammatory cytokines, including *IL-1β*, *IL-12a*, *IL-12b (IL-12/23 p40)*, *IL-6* and *IL-23a*, decreased obviously upon spermidine treatment (Figure 4A). It has been widely accepted that spermidine is a potent autophagy inducer. So, the genes enriched in phagosome pathway were induced by spermidine in IFN-DC (Figure 4A). More importantly, we found that the FOXO pathway, which was reported coordinating autophagy, metabolism, and energy homeostasis, was activated by spermidine, whereas it was inhibited by TLR ligand stimulation (Figure 4A).

The FOXO transcription factors (FOXO1, FOXO3, FOXO4, and FOXO6) are involved in a wide range of cellular processes. Among them, FOXO3 is particularly important for metabolic adaption and immune response (Martins et al., 2016). FOXO3 is tightly regulated by the metabolic state of the cell. Under conditions of high glucose, AKT phosphorylates FOXO3 at three conserved residues, Thr32, Ser253, and Ser315. This leads to FOXO3 binding to 14-3-3, exposure of the nuclear localization signal, transporting to the cytosol and being degraded, causing reduced expression of FOXO3 target genes (Zhang et al., 2018). When ATP is low, FOXO3 is phosphorylated by AMPK at Ser413 and exhibits increased activity (Lee et al., 2013; Zhang et al., 2018). *Foxo3a*-deficient DCs express higher levels of proinflammatory cytokines (Dejean et al., 2009; Lee et al., 2013; Litvak et al., 2012; Thompson et al., 2015; Zhang et al., 2018). For these reasons, we hypothesized that FOXO3 might be the critical transcriptional factor in the process.

To test our hypothesis, moDCs were stimulated with IFN-α and IFN-DCs were stimulated with R837, together with spermidine or not. The phosphorylation levels of AKT and FOXO3 were detected. On the one hand, AKT was activated by IFN priming and TLR ligand stimulation, whereas the activation was hampered by spermidine (Figure 4B). Then, activated AKT phosphorylates FOXO3 at Ser253, whereas it was suppressed by spermidine (Figure 4B). On the other hand, the activated form of FOXO3 phosphorylated at Ser413 decreased during IFN priming, accompanied by suppressed AMPK signaling (Figures 3C and 4B). By contrast, spermidine restored the activity of AMPK pathway and induced increased phosphorylation levels of FOXO3 at Ser413 in the presence of R837 (Figures 3C and 4B). Therefore, spermidine induced the activated form of FOXO3 (p-FOXO3 at Ser413) and reduced the inactive form of FOXO3 (p-FOXO3 at Ser253) during IFN-DC activation (Figure S4A and S4B). The end result was that spermidine caused FOXO3 to localize in the nucleus where it was active, as we demonstrated by separating the cytoplasmic and nuclear fractions of DCs, and finding that spermidine increased the amount of FOXO3 in the nucleus (Figure 4C). Finally, the activation of NF-κB was suppressed by spermidine (Figure 4B).

To verify that FOXO3 mediates the anti-inflammatory effect of spermidine, moDCs derived from WT or *Foxo3a*-deficient mice were primed with IFN-α for 24 h, and then cultured with R837, together with or without spermidine for 24 h, respectively. The knockout efficiency has been confirmed (Figure S4C). Compared with control, *Foxo3a*-deficient IFN-DCs showed higher expression levels of TNF-α, IL-6, and IL-12/23 p40. Addition of spermidine led to a reduction of 63.8%, 72.6%, and 70.8% in the expression of TNF-α, IL-6, and IL12/23 p40 in wild-type IFN-DCs, whereas only 18.8%, 26.9%, and 16.1% reduction were detected in *Foxo3a*$^{-/-}$ IFN-DCs, respectively (Figure 4D). Thus, the anti-inflammatory effect of spermidine was greatly weakened in *Foxo3a*$^{-/-}$ IFN-DCs.

Taken together, FOXO3 adapts to metabolic changes in DCs by changing phosphorylation levels at different sites and ultimately mediates the anti-inflammatory effect of spermidine.

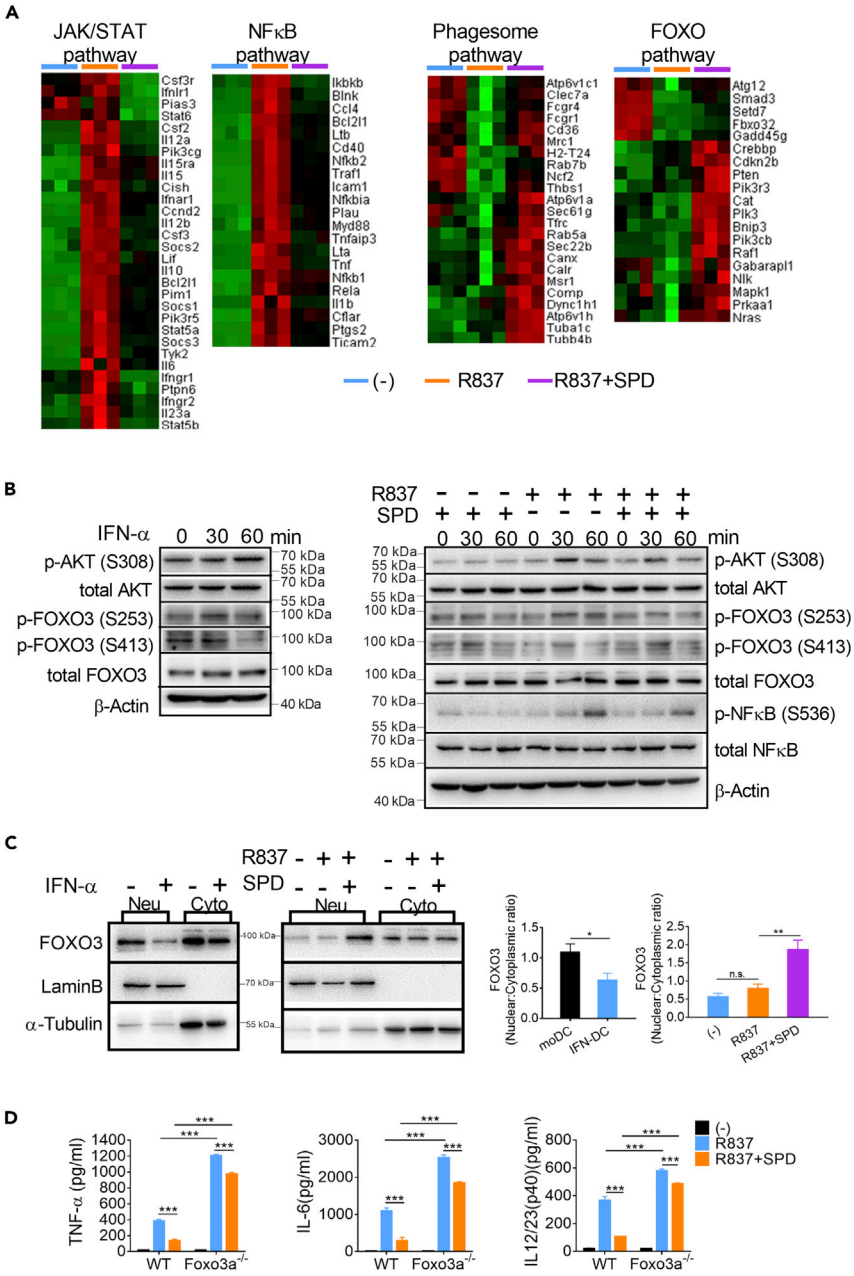

Figure 4. FOXO3 Mediates the Anti-inflammatory Effect of Spermidine

(A) IFN-DCs were cultured with R837, together with or without spermidine (SPD) for 18 h. Cells were collected and the mRNA expression was detected by RNA-seq (n = 3). Changed genes enriched in JAK/STAT, NF-κB, phagosome, and FOXO pathways are shown.

(B) MoDCs were treated with IFN-α for 30 or 60 min. IFN-DCs were treated with R837 or R837 and spermidine for 30 or 60 min. The levels of proteins were analyzed by immunoblot. β-ACTIN was used as the internal loading control. Data are representative of three independent experiments.

(C) MoDCs were treated with IFN-α for 18 h. IFN-DCs were treated with R837 or R837 and spermidine for 18 h. Then, cells were collected, separated into nuclear and cytoplasmic fractions, and analyzed by immunoblot. LaminB and α-Tubulin were used as loading controls. The nuclear/cytoplasmic ratios were calculated by (nuclear FOXO3/LaminB)/(cytoplasmic FOXO3/α-Tubulin). Data are representative of three independent experiments. Error bars represent SEM.

(D) The levels of TNF-α, IL-6, and IL-12/23 p40 released by WT and *Foxo3*$^{-/-}$ IFN-DC stimulated with 10 μg/mL R837 in the presence or absence of spermidine for 24 h (n = 3). Data are representative of three independent experiments. Error bars represent SEM. P values were determined by two-tailed unpaired t test, *p < 0.05, **p < 0.01, ***p < 0.001. n.s., not significant.

Administration of Spermidine Ameliorates the Pathological Phenotype of IMQ-Induced Psoriasis-like Mice

Psoriasis is one of the most common immune-mediated chronic inflammatory skin disorders with high levels of IFN-α production and infiltration of moDCs in skin plaque in the early stage (Lowes et al., 2014; Singh et al., 2016; Terhorst et al., 2015). The role of type I IFNs and TLR7 has been studied more extensively in IMQ-induced psoriatic mice model than in other autoimmune disease models. TLR7 is essential for the full progression of psoriasis during the 6 days induction, whereas the type I IFNs are largely independent of plaque formation (Wohn et al., 2013). However, auto- and paracrine signals via type I IFN are essential to mediate the innate systemic proinflammatory cytokine response after topical IMQ application, as induction of the early systemic proinflammatory cytokines IFN-α, IL-22, and IL-6 was found significantly lower in *IFNAR*$^{-/-}$ mice (Wohn et al., 2013). The synergistic effect of IMQ and IFN-a was proven to cause the activation of moDCs, leading to the production of TNF-a, IL-6, and IL-23 required for Th17 differentiation (Ueyama et al., 2014). Therefore, the regulation of spermidine on the function of IFN-DC *in vivo* can be evaluated by detecting skin plaque formation and systematic inflammation including splenomegaly and cytokine production in serum.

Repetitive application of IMQ onto wild-type mouse skin led to psoriasiform inflammation with significant thickening, redness, and scaling caused by keratinocyte hyperproliferation and leukocyte infiltration into the skin (Figures 5A–5C). High levels of IFN-α were detected as early as 8 h post first IMQ application when the mRNA levels of TLR7 remained low 2 days after induction (Figure S5A and S5B). The result that expression of TLR7 was significantly induced in dermal moDCs 4 days after induction suggests that the skin lesion sites might experience a local IFN-α priming process. By contrast, mice injected intraperitoneally with spermidine showed less skin inflammation, exhibiting less thickening, redness, and scaling (Figures 5B and 5C). The induction of TLR7 was also suppressed by spermidine (Figure S5C). Hematoxylin and eosin (H&E)-stained back skin and ear sections from spermidine-treated mice displayed a reduction in epidermal and dermal thickness during the course of disease (Figures 5D and 5E). On day 6, the peak of psoriasis-like changes, we observed that the splenomegaly of mice in the spermidine-treated group was much less obvious than that in the control group (Figure S6A). In line with this, reduced mRNA levels of *IL-23a*, *TNF-α*, *IL-6*, and *IL-17a* were observed in the skin lesions of the spermidine-injected mice (Figure 5F). Notably, we found that the levels of IL-23, TNF-α, IL-6, and IL-17A in serum were inhibited by spermidine in the early stage (Figure 5F).

To further determine the inflammatory cell infiltration in dermis from the spermidine-treated or control groups, we obtained dermal single-cell suspensions and analyzed the percentages of different immune cell subsets. Results demonstrated that the percentages of $CD45^+$ immune cells, including moDCs ($CD45^+MHCII^{hi}Ly6C^{-/lo}CD64^-CD11c^+CD11b^+$), neutrophils ($CD45^+Ly6G^+$), and IL-$17^+\gamma\delta$T cells ($CD45^+CD3^+$ $\gamma\delta TCR^+IL\text{-}17A^+$), reduced in the dermis of the spermidine-treated group (Figures 5G and S7). Similarly, the number of splenocytes, including $ly6C^{hi}$ monocytes, macrophages, neutrophils, B cells, pDCs, $CD8\alpha^-$ cDCs, $CD4^+$ T cells, and $CD8^+$ T cells, decreased in the spermidine-treated group after IMQ application (Figures S6B and S6C). Therefore, spermidine can prevent the immunopathological changes in psoriasis and effectively ameliorate disease severity.

IFN-DC Participates in the Anti-Psoriasis Process of Spermidine

To address that the role of spermidine is IFN-DC intrinsic, we used antibody-mediated depletion of monocytes in mice (Figure 6A). The available antibodies allowed us to deplete $Ly6C^{hi}$ monocytes plus neutrophils or neutrophils alone effectively (Figure S8A). Depleting neutrophils alone had little effect on the inflammatory response and psoriasis progression (Figures 6B–6E), which was consistent with previous report (Singh et al., 2016). The additional depletion of $Ly6C^{hi}$ monocytes led to a loss of peripheral circulating monocytes and was accompanied by a significant decrease in redness, scaling, and epidermal and dermal thickness (Figures 6B–6E), as well as protein levels of inflammatory cytokines, including IL-23, TNF-α, IL-6, and IL-17A (Figure 6F). More importantly, there was no difference in the severity of psoriasis-like skin inflammation between IMQ-painted control mice (Anti-Gr1+IMQ) and spermidine-treated mice (Anti-Gr1+IMQ + SPD) after $Ly6C^{hi}$ monocytes depletion, as they showed a similar decrease in epidermal and dermal thicknesses (Figures 6D and 6E). The difference in protein levels of IL-23, TNF-α, and IL-17A disappeared (Figure 6F). Meanwhile, there was no difference in the numbers of splenic macrophages, neutrophils, and $CD4^+$ T cells between control (Anti-Gr1+IMQ) and spermidine-treated mice (Anti-Gr1+IMQ + SPD) after monocyte depletion (Figure S8B). And the gaps in the different numbers of splenic B cells, pDCs,

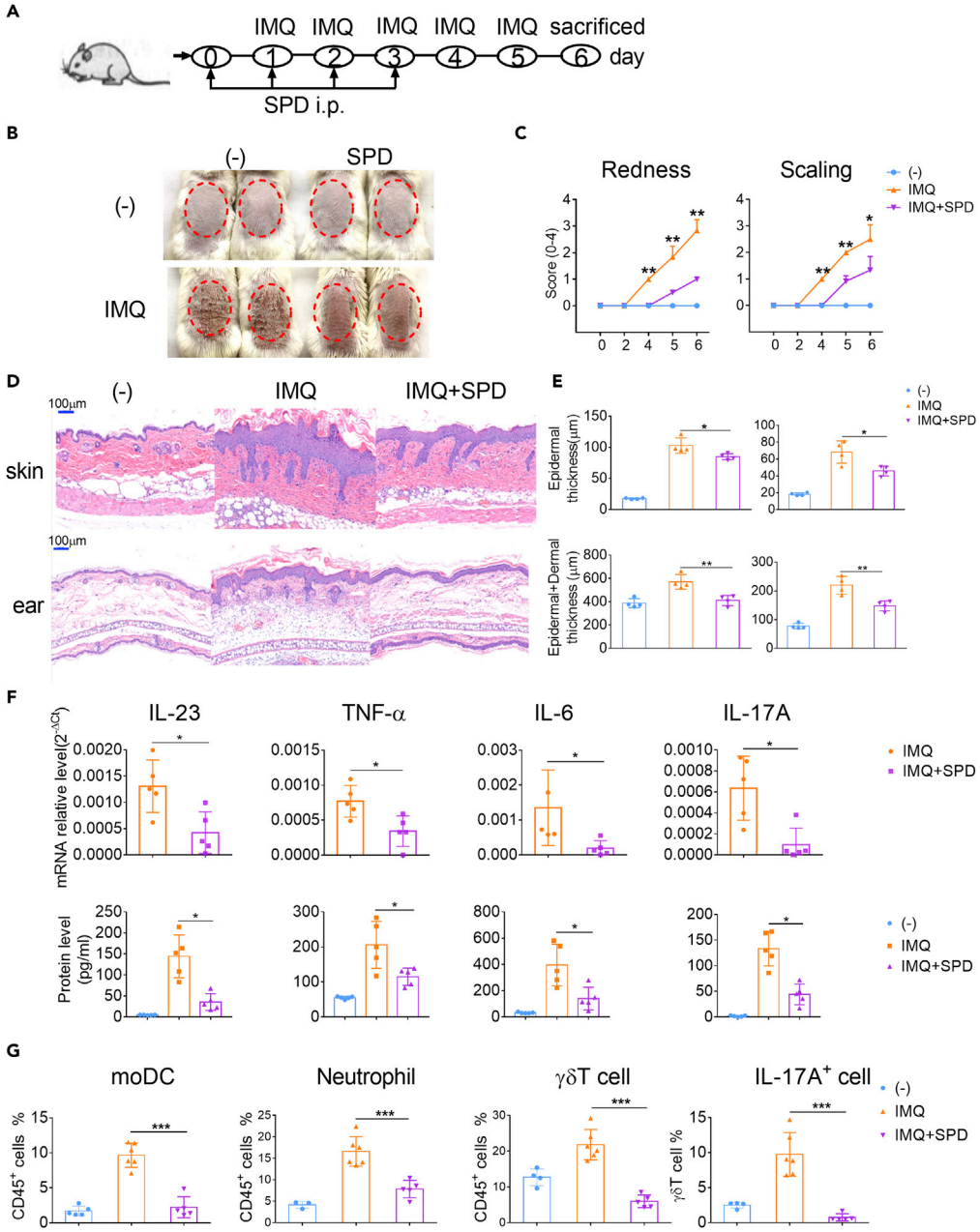

Figure 5. Administration of Spermidine Ameliorates the Pathological Phenotype of IMQ-Induced Psoriasis-like Mice

(A) Schematic diagram for IMQ application and intraperitoneal administration of spermidine (SPD).

(B) Phenotypic presentation of skin lesions of representative mice on day 6 (n = 5).

(C) Increase in back skin redness and scaling (n = 6).

(D) Representative H&E-stained sections of the back skin and ear on day 6 are shown. Magnification 100× (scale bars represent 100 μm).

(E) Skin epidermal (upper left) and epidermal plus dermal thickness (lower left), and ear epidermal (upper right) and epidermal plus dermal thickness (lower right) (n = 4).

(F) The mRNA expression of *IL-23a*, *TNF-α*, *IL-6*, and *IL-17a* in skin plaque on day 4 and the protein levels of IL-23, TNF-α, IL-6, and IL-17A in serum on day 2 (n = 5). The expression of mRNA was normalized to *β-actin* mRNA by calculating $2^{-\Delta Ct}$.

(G) Statistical data of the skin infiltration of moDCs ($CD45^+MHCII^+Ly6C^{-/lo}CD64^-CD11c^+CD11b^+$), neutrophils ($CD45^+Ly6G^+$), γδT cells ($CD45^+CD3^+\gamma\delta TCR^+$), and IL-17A$^+$ γδT cells ($CD45^+CD3^+\gamma\delta TCR^+IL\text{-}17A^+$) (n = 5). Each dot represents a mouse. Data are representative of three independent experiments and shown as mean ± SEM. P values were determined by two-tailed unpaired t test. *p < 0.05, **p < 0.01, ***p < 0.001.

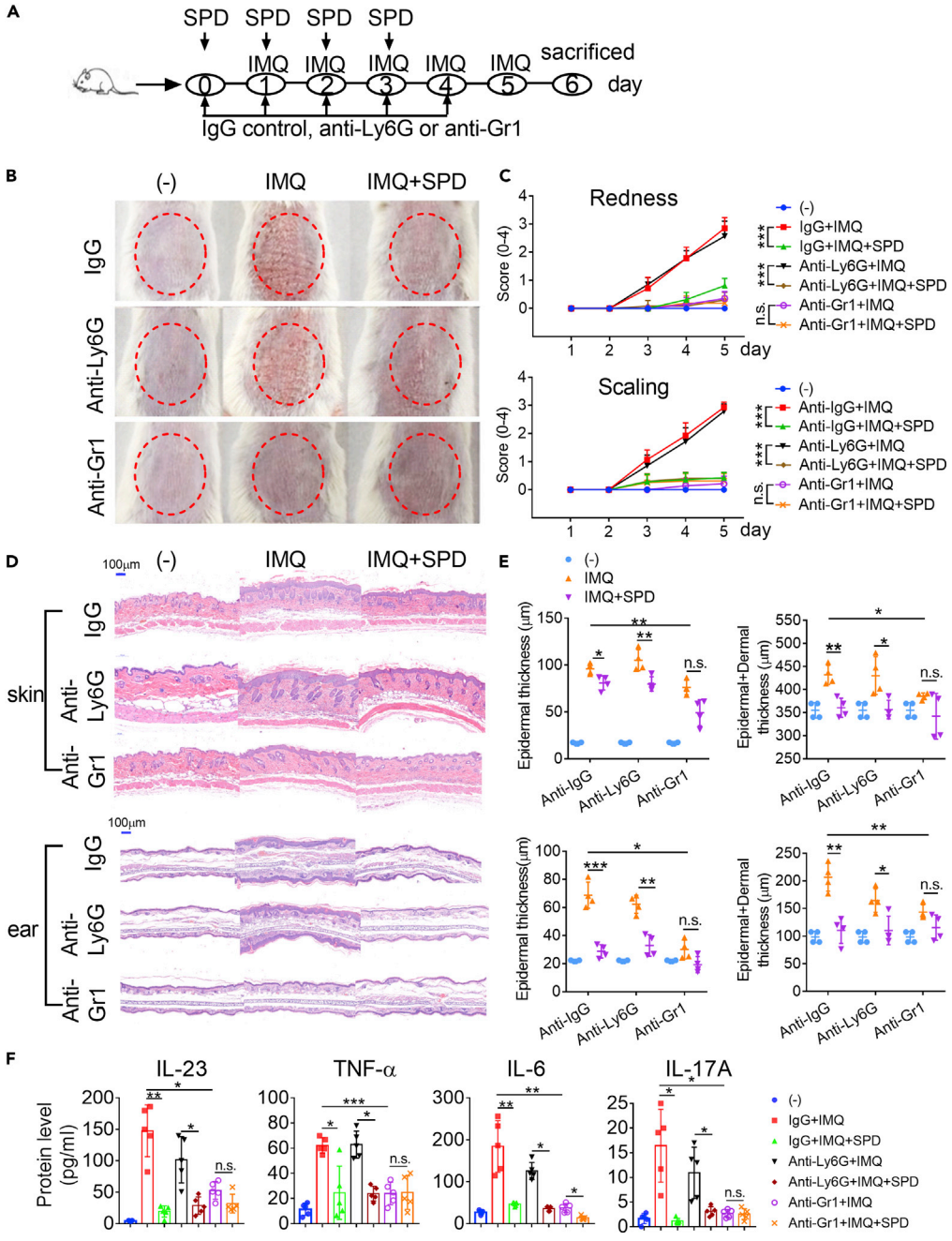

Figure 6. IFN-DC Participates in the Anti-Psoriasis Process of Spermidine

(A) Schematic diagram for IMQ application and depletion of neutrophils alone (Anti-Ly6G) or monocytes plus neutrophils (Anti-Gr1) in mice.

(B) Phenotypic presentation.

(C) Increase in redness score and scaling score (n = 5).

(D and E) (D) H&E staining of skin lesions of representative mice on day 5. Magnification 100× (scale bars represent 100 μm). (E, upper) Skin epidermal and epidermal plus dermal thickness, and (lower) ear epidermal and epidermal plus dermal thickness on day 5 (n = 4).

(F) The protein levels of IL-23, TNF-α, IL-6, and IL-17A in serum (n = 5). Each dot represents a mouse.

All data are representative of three independent experiments and shown as mean ± SEM. P values were determined by an unpaired t test or two-way ANOVA. *p < 0.05, **p < 0.01, ***p < 0.001, n.s. not significant.

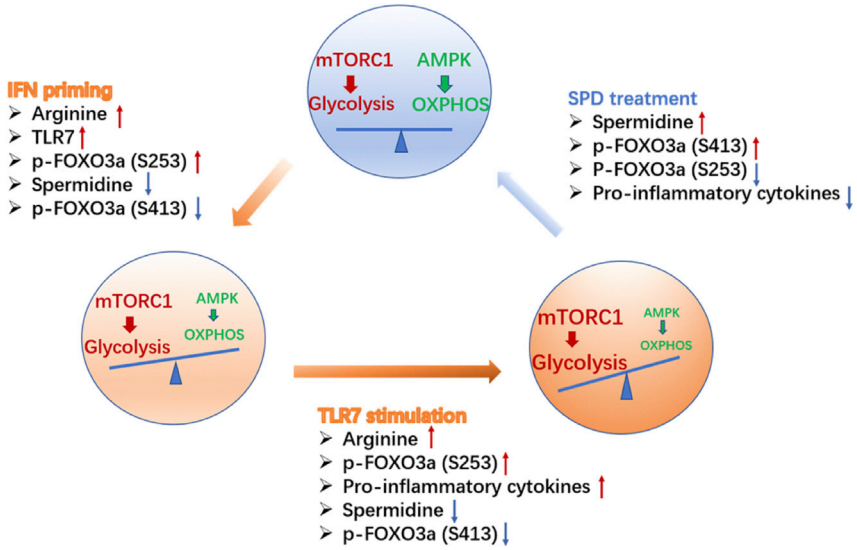

Figure 7. Regulation Model

IFN priming results in reduced spermidine, accompanied by increased glycolysis and decreased oxidative phosphorylation, facilitating DC responding to weak signal. TLR7 ligand stimulation further aggravates the metabolic shift. Addition of spermidine restrains the process and prevents DC from overactivation in autoimmune disease. The transcription factor FOXO3 adapts its activity to the metabolic change and mediates the anti-inflammatory effect of spermidine by altering phosphorylation levels at different sites.

$CD8\alpha^-$ cDCs, and $CD8^+$ T cells also narrowed. The fact that depletion of monocytes eliminated the difference in the therapeutic effect of spermidine on the development of psoriasis suggests that the function of spermidine is partially IFN-DC dependent.

Taken together, these results indicate that spermidine changes the metabolic status of DC by regulating key metabolic pathways, thereby affecting the autoimmune response *in vivo*, suggesting a treatment strategy for IFN-DC-related autoimmune diseases, including psoriasis and SLE (Figure 7).

DISCUSSION

In this study, we investigated amino acid metabolism by screening changes in amino acids and their derivates during IFN priming and TLR7 agonist treatment. Among changed amino acids, L-arginine and its derivatives were particularly important. IFN priming led to decreased spermidine. TLR7 agonist exacerbated the change. Spermidine supplement enforced metabolic quiescence in IFN-DC and reduced the IFN-DC production of pro-inflammatory cytokines *in vitro* and *in vivo*. Administration of spermidine ameliorated the pathological phenotype and systematic inflammation of IMQ-induced psoriasis-like mice, suggesting the spermidine metabolism pathway could be considered as a target for autoimmune disease treatment.

IFN-α promotes the induction of immune responses, including auto-reactive responses. It was found promoting the chromatinic opening of inflammatory NF-κB target genes, thereby potentiating TNF function (Park et al., 2017). By inducing increased fatty acid oxidation (FAO) and OXPHOS, type I IFNs facilitate full pDC activation (Wu et al., 2016). Here, we observed that IFN priming led to the reduction in spermidine level by suppressing the expression of enzymes involved in polyamine metabolism. As a result, DCs become sensitive to weak signals, such as self-RNA complexes. Therefore, the effect of IFN-α on polyamine metabolism might be a different mechanism by which it promotes autoimmune responses.

Tlr7$^{-/-}$ mice were found to have obviously improved symptoms during a 6-day induction by IMQ (Farkas and Kemeny, 2012; Ueyama et al., 2014), suggesting an indispensable role for TLR7 in the IMQ-induced psoriatic mice model. The function of spermidine on the improvement of pathological plaque formation may indicate its suppression of TLR7 activation in moDCs. Significant elevation of IFN-α was detected 8 h after IMQ application, whereas the mRNA levels of *TLR7* were induced on day 4 (Figure S5). Thus, the inhibitory effects of spermidine on TLR7 expression and systematic inflammatory cytokine production

may suggest its dual inhibition of both IFN priming and TLR7 activation, inferred from previous reports. Moreover, spermidine exerting its protective effects is more likely through IFN-DC, as antibody deletion of moDC reduced the differences in symptoms and cytokines between the control group and spermidine-treated group. However, our study did not rule out the possibility that it works by acting on other cell subsets.

FOXO3 has been reported to be closely related to inflammatory cytokine production and autoimmune diseases and to limit the inflammatory sequelae of viral infections. A noncoding polymorphism in *Foxo3a* (rs12212067: T > G) was identified at which the minor (G) allele, despite not being associated with disease susceptibility, is associated with a milder course of Crohn's disease and rheumatoid arthritis and with an increased risk of severe malaria (Lee et al., 2013). Notably, *Foxo3a* was found to be a susceptibility gene of psoriatic patients (Pektas et al., 2018), strengthening the critical role for FOXO3 in autoimmune diseases. We demonstrated that spermidine was an activator of FOXO3. Fine-tuning spermidine level will help improve many autoimmune symptoms caused by FOXO3 dysfunction. Differently, the degradation of FOXO3 was reported to protect $CD8^+$ DC from oxidative stress in non-obese diabetic mice, indicating that FOXO3 may play different roles in different DC subsets or autoimmune diseases (Fallarino Serreze et al., 2004). More in-depth disease model study by using foxo3a conditional knockout mice will help clarify these questions. Besides, the NF-κB pathway might also be involved in the regulation, as both RNA sequencing and immunoblots supported that the NF-κB pathway was inhibited in spermidine-treated groups.

Spermidine displays pleiotropic effects that include anti-inflammatory properties, antioxidant functions, and enhancement of mitochondrial metabolic function and respiration, as well as improved proteostasis and chaperone activity (Farkas and Kemeny, 2012; Madeo et al., 2018; Mondanelli et al., 2017; Puleston et al., 2019). Polyamine biosynthesis modulates mitochondrial metabolism through eIF5A hypusination, induces efficient expression of some mitochondrial enzymes, and facilitates OXPHOS-dependent macrophage alternative activation without affecting aerobic glycolysis-dependent macrophage classical activation. We also noticed that spermidine supplement led to the trend of increasing OXPHOS in IFN-DC during R837 stimulation (Figure 3A). Since the metabolic regulation varies by cell and microenvironment, the different regulation of polyamines on glycolysis may be due to different cell types. Spermidine supplement alleviates experimental autoimmune encephalomyelitis through inducing inhibitory macrophages (Yang et al., 2016), supporting the protective role of spermidine in autoimmune disease. Differently, spermidine could directly improve the generation and function of memory lymphocytes, favoring the chemotherapeutic efficiency against autophagy-competent cancers (Madeo et al., 2018). Here, we highlight its critical role in IFN-related autoimmune diseases. Consistent with this, spermidine and spermine in plasma of patients with SLE and fever were found to be decreased (Kim et al., 2018).

Generally, metabolite levels can be influenced without genetic manipulations, offering the possibility for therapeutic applications. Given the importance of polyamine metabolism during infection, cancer, and autoimmune diseases, there is a clinical need for approaches to modify it. The verified mechanism for spermidine function in DC provides a way to alter the immunometabolism. Additionally, our dataset on the dynamics of the amino acids and polyamines during the IFN-priming and activation of DCs constitute a framework for future studies addressing the complex interplay between metabolism and cellular functions.

Limitations of the Study

In this study, we demonstrated that intraperitoneal injection of spermidine alleviated the progression of psoriasis. To verify that spermidine functions by acting on moDCs, we adopted the strategy of antibody-mediated monocyte depletion *in vivo* and found that there was almost no significant difference between control and spermidine-treated groups, indicating that spermidine might function through moDCs. However, our study did not rule out that spermidine worked by acting on other cells. Besides TLR7 ligand stimulation, we also tested other TLR ligand stimuli. We found that spermidine could inhibit the activation of moDCs by TLR9 ligand stimulation, whereas TLR4 ligand stimulation was not affected. Further study will help to clarify why the function of spermidine varies with the type of stimulus.

METHODS

All methods can be found in the accompanying Transparent Methods supplemental file.

SUPPLEMENTAL INFORMATION

Supplemental Information can be found online at https://doi.org/10.1016/j.isci.2019.100807.

ACKNOWLEDGMENT

This study was supported by grants from National Natural Science Foundation of China (No. 31600706, 81974252, 81421001, 81571575, 81771737) and Sanming Project of Medicine in Shenzhen (SZSM201602087).

AUTHOR CONTRIBUTIONS

N.S. and H.Z. designed the project. G.L. performed the experiments, and G.L., Y.M., J.L., and H.Z. analyzed the data. H.Z. and X.Y. analyzed the bioinformatics data. Y.M. established the mouse model. H.D. and Q.G. collected the mouse samples. G.L., H.Z., and N.S. prepared the manuscript.

DECLARATION OF INTERESTS

The authors declare no competing interests.

Received: August 18, 2019
Revised: November 27, 2019
Accepted: December 23, 2019
Published: January 24, 2020

REFERENCES

Babicova, A., Havlinova, Z., Pejchal, J., Tichy, A., Rezacova, M., Vavrova, J., and Chladek, J. (2011). Early changes in L-arginine-nitric oxide metabolic pathways in response to the whole-body gamma irradiation of rats. Int. J. Radiat. Biol. *87*, 1067–1073.

Blanco, P., Palucka, A.K., Gill, M., Pascual, V., and Banchereau, J. (2001). Induction of dendritic cell differentiation by IFN-alpha in systemic lupus erythematosus. Science *294*, 1540–1543.

Dejean, A.S., Beisner, D.R., Ch'en, I.L., Kerdiles, Y.M., Babour, A., Arden, K.C., Castrillon, D.H., DePinho, R.A., and Hedrick, S.M. (2009). Transcription factor Foxo3 controls the magnitude of T cell immune responses by modulating the function of dendritic cells. Nat. Immunol. *10*, 504–513.

Durai, V., and Murphy, K.M. (2016). Functions of murine dendritic cells. Immunity *45*, 719–736.

Everts, B., and Pearce, E.J. (2014). Metabolic control of dendritic cell activation and function: recent advances and clinical implications. Front. Immunol. *5*, 203.

Fallarino Serreze, D.V., Grohmann, U., and Puccetti, P. (2004). CTLA-4-Ig activates forkhead transcription factors and protects dendritic cells from oxidative stress in nonobese diabetic mice. J. Exp. Med. *200*, 1051–1062.

Farkas, A., and Kemeny, L. (2012). Monocyte-derived interferon-alpha primed dendritic cells in the pathogenesis of psoriasis: new pieces in the puzzle. Int. Immunopharmacol. *13*, 215–218.

Ganguly, D. (2018). Do type I interferons link systemic autoimmunities and metabolic syndrome in a pathogenetic continuum? Trends Immunol. *39*, 28–43.

Geiger, R., Rieckmann, J.C., Wolf, T., Basso, C., Feng, Y., Fuhrer, T., Kogadeeva, M., Picotti, P., Meissner, F., Mann, M., et al. (2016). L-arginine modulates T cell metabolism and enhances survival and anti-tumor activity. Cell *167*, 829–842 e813.

Kim, H.A., Lee, H.S., Shin, T.H., Jung, J.Y., Baek, W.Y., Park, H.J., Lee, G., Paik, M.J., and Suh, C.H. (2018). Polyamine patterns in plasma of patients with systemic lupus erythematosus and fever. Lupus *27*, 930–938.

Lee, J.C., Espeli, M., Anderson, C.A., Linterman, M.A., Pocock, J.M., Williams, N.J., Roberts, R., Viatte, S., Fu, B., Peshu, N., et al. (2013). Human SNP links differential outcomes in inflammatory and infectious disease to a FOXO3-regulated pathway. Cell *155*, 57–69.

Litvak, V., Ratushny, A.V., Lampano, A.E., Schmitz, F., Huang, A.C., Raman, A., Rust, A.G., Bergthaler, A., Aitchison, J.D., and Aderem, A. (2012). A FOXO3-IRF7 gene regulatory circuit limits inflammatory sequelae of antiviral responses. Nature *490*, 421–425.

Locke, M., Ghazaly, E., Freitas, M.O., Mitsinga, M., Lattanzio, L., Lo Nigro, C., Nagano, A., Wang, J., Chelala, C., Szlosarek, P., et al. (2016). Inhibition of the polyamine synthesis pathway is synthetically lethal with loss of argininosuccinate synthase 1. Cell Rep. *16*, 1604–1613.

Lowes, M.A., Suarez-Farinas, M., and Krueger, J.G. (2014). Immunology of psoriasis. Annu. Rev. Immunol. *32*, 227–255.

Madeo, F., Eisenberg, T., Pietrocola, F., and Kroemer, G. (2018). Spermidine in health and disease. Science *359*, eaan2788.

Malissen, B., Tamoutounour, S., and Henri, S. (2014). The origins and functions of dendritic cells and macrophages in the skin. Nat. Rev. Immunol. *14*, 417–428.

Martins, R., Lithgow, G.J., and Link, W. (2016). Long live FOXO: unraveling the role of FOXO proteins in aging and longevity. Aging Cell *15*, 196–207.

Merad, M., Sathe, P., Helft, J., Miller, J., and Mortha, A. (2013). The dendritic cell lineage: ontogeny and function of dendritic cells and their subsets in the steady state and the inflamed setting. Annu. Rev. Immunol. *31*, 563–604.

Mohty, M., Vialle-Castellano, A., Nunes, J.A., Isnardon, D., Olive, D., and Gaugler, B. (2003). IFN-alpha skews monocyte differentiation into Toll-like receptor 7-expressing dendritic cells with potent functional activities. J. Immunol. *171*, 3385–3393.

Mondanelli, G., Bianchi, R., Pallotta, M.T., Orabona, C., Albini, E., Iacono, A., Belladonna, M.L., Vacca, C., Fallarino, F., Macchiarulo, A., et al. (2017). A relay pathway between arginine and tryptophan metabolism confers immunosuppressive properties on dendritic cells. Immunity *46*, 233–244.

O'Neill, L.A., and Pearce, E.J. (2016). Immunometabolism governs dendritic cell and macrophage function. J. Exp. Med. *213*, 15–23.

Park, S.H., Kang, K., Giannopoulou, E., Qiao, Y., Kang, K., Kim, G., Park-Min, K.H., and Ivashkiv, L.B. (2017). Type I interferons and the cytokine TNF cooperatively reprogram the macrophage epigenome to promote inflammatory activation. Nat. Immunol. *18*, 1104–1116.

Pearce, E.J., and Everts, B. (2015). Dendritic cell metabolism. Nat. Rev. Immunol. *15*, 18–29.

Pektas, S.D., Dogan, G., Edgunlu, T.G., Karakas-Celik, S., Ermis, E., and Tekin, N.S. (2018). The role

of forkhead box class O3A and SIRT1 gene variants in early-onset psoriasis. Indian J. Dermatol. *63*, 208–214.

Postat, J., Olekhnovitch, R., Lemaitre, F., and Bousso, P. (2018). A metabolism-based quorum sensing mechanism contributes to termination of inflammatory responses. Immunity *49*, 654–665 e655.

Puleston, D.J., Buck, M.D., Klein Geltink, R.I., Kyle, R.L., Caputa, G., O'Sullivan, D., Cameron, A.M., Castoldi, A., Musa, Y., Kabat, A.M., et al. (2019). Polyamines and eIF5A hypusination modulate mitochondrial respiration and macrophage activation. Cell Metab. *30*, 352–363.e8.

Rodriguez-Pla, A., Patel, P., Maecker, H.T., Rossello-Urgell, J., Baldwin, N., Bennett, L., Cantrell, V., Baisch, J., Punaro, M., Gotte, A., et al. (2014). IFN priming is necessary but not sufficient to turn on a migratory dendritic cell program in lupus monocytes. J. Immunol. *192*, 5586–5598.

Santini, S.M., Lapenta, C., Donati, S., Spadaro, F., Belardelli, F., and Ferrantini, M. (2011). Interferon-alpha-conditioned human monocytes combine a Th1-orienting attitude with the induction of autologous Th17 responses: role of IL-23 and IL-12. PLoS One *6*, e17364.

Schwartz, D.M., Bonelli, M., Gadina, M., and O'Shea, J.J. (2016). Type I/II cytokines, JAKs, and new strategies for treating autoimmune diseases. Nat. Rev. Rheumatol. *12*, 25–36.

Shortman, K., and Naik, S.H. (2007). Steady-state and inflammatory dendritic-cell development. Nat. Rev. Immunol. *7*, 19–30.

Singh, T.P., Zhang, H.H., Borek, I., Wolf, P., Hedrick, M.N., Singh, S.P., Kelsall, B.L., Clausen, B.E., and Farber, J.M. (2016). Monocyte-derived inflammatory Langerhans cells and dermal dendritic cells mediate psoriasis-like inflammation. Nat. Commun. *7*, 13581.

Terhorst, D., Chelbi, R., Wohn, C., Malosse, C., Tamoutounour, S., Jorquera, A., Bajenoff, M., Dalod, M., Malissen, B., and Henri, S. (2015). Dynamics and transcriptomics of skin dendritic cells and macrophages in an imiquimod-induced, biphasic mouse model of psoriasis. J. Immunol. *195*, 4953–4961.

Thompson, M.G., Larson, M., Vidrine, A., Barrios, K., Navarro, F., Meyers, K., Simms, P., Prajapati, K., Chitsike, L., Hellman, L.M., et al. (2015). FOXO3-NF-kappaB RelA protein complexes reduce proinflammatory cell signaling and function. J. Immunol. *195*, 5637–5647.

Ueyama, A., Yamamoto, M., Tsujii, K., Furue, Y., Imura, C., Shichijo, M., and Yasui, K. (2014). Mechanism of pathogenesis of imiquimod-induced skin inflammation in the mouse: a role for interferon-alpha in dendritic cell activation by imiquimod. J. Dermatol. *41*, 135–143.

Wohn, C., Ober-Blobaum, J.L., Haak, S., Pantelyushin, S., Cheong, C., Zahner, S.P., Onderwater, S., Kant, M., Weighardt, H., Holzmann, B., et al. (2013). Langerin(neg) conventional dendritic cells produce IL-23 to drive psoriatic plaque formation in mice. Proc. Natl. Acad. Sci. U S A *110*, 10723–10728.

Worbs, T., Hammerschmidt, S.I., and Forster, R. (2017). Dendritic cell migration in health and disease. Nat. Rev. Immunol. *17*, 30–48.

Wu, D., Sanin, D.E., Everts, B., Chen, Q., Qiu, J., Buck, M.D., Patterson, A., Smith, A.M., Chang, C.H., Liu, Z., et al. (2016). Type 1 interferons induce changes in core metabolism that are critical for immune function. Immunity *44*, 1325–1336.

Yang, Q., Zheng, C., Cao, J., Cao, G., Shou, P., Lin, L., Velletri, T., Jiang, M., Chen, Q., Han, Y., et al. (2016). Spermidine alleviates experimental autoimmune encephalomyelitis through inducing inhibitory macrophages. Cell Death Differ. *23*, 1850–1861.

Zhang, Y., Paikari, A., Sumazin, P., Ginter Summarell, C.C., Crosby, J.R., Boerwinkle, E., Weiss, M.J., and Sheehan, V.A. (2018). Metformin induces FOXO3-dependent fetal hemoglobin production in human primary erythroid cells. Blood *132*, 321–333.

iScience, Volume *23*

Supplemental Information

Spermidine Suppresses Inflammatory DC Function by Activating the FOXO3 Pathway and Counteracts Autoimmunity

Guanhua Li, Huihua Ding, Xiang Yu, Yao Meng, Jun Li, Qiang Guo, Haibo Zhou, and Nan Shen

Transparent Methods

Mice

All mouse studies were approved by the Animal Care Committee of Renji Hospital. The C57BL/6J and BALB/c mice were purchased from Slack Company. *Foxo3a*$^{-/-}$ mice were generated via CRISPR/Cas9 system. Briefly, sgRNAs-targeting the introns on both sides of the exon 2 of *Foxo3a* were respectively constructed and transcribed in vitro. Then Cas9 mRNA and sgRNA will be co-injected into zygotes. Thereafter, the zygotes were transferred into the oviduct of pseudo pregnant ICR females at 0.5 dpc. And F0 mice was birthed after 19~21 days of transplantation. All the off springs of ICR females (F0 mice) were examined by PCR and sequencing of tail DNA. Finally, positive F0 mice were crossed with C57BL/6J mice to build up heterozygous mice. Mice were bred and housed under SPF conditions. All mice were male at 8-10 weeks of age.

Metabolomics

MoDCs were incubated in the presence or absence of IFN-α. After 24 hours, cells were collected to perform extraction of metabolites. IFN-DC were incubated with R837 (InvivoGen), in presence of absence of spermidine (Sigma-Aldrich). After 0.5, 4 and 16 hours, samples were collected to perform extraction of metabolites. Amino acids were measured in cell samples that were previously stored at −80°C using a quantitative UPLC-MS/MS platform (ACQUITY UPLC-Xevo TQ-S, Waters Corp., Milford, MA, USA) according to previously published methods (Chen et al., 2016a; Chen et al., 2016b). All chromatographic separations were performed with an ACQUITY BEH C18 column VanGuard pre-column (2.1×5 mm) and analytical column (2.1×100 mm). The elution solvents were water with 0.2% formic acid (A) and acetonitrile with 0.2% formic acid (B). The flow rate was 500μl/min with the following mobile phase gradient: 0–0.38 min (1% B), 0.38–3 min (1–15% B), 3–5.4 min (15–70% B), 5.5–5.9 min (100% B), and 5.9–6.6 min (100-1% B). The cone and collision energy for each amino acid used the optimized settings from QuanOptimize application manager. All of the amino acid standards were obtained from Sigma-Aldrich (St. Louis, MO, USA), and 14 stable isotope- labeled standards were obtained from Cambridge Isotope Laboratories, Inc. (Tewksbury, MA, USA). The standards and stable isotope-labeled standards were accurately weighed and prepared in water to obtain individual stock solution at a concentration of 5.0 or 20.0 mM. The stock solution of individual amino acids was mixed and prepared to obtain a series of amino acid calibrators at a final concentration of 5000, 2500, 500, 150, 10, 2.5, or 1 nM. The raw data generated by UPLC-MS/MS were then processed using the QuanMET software (v1.0, Metabo-Profile, Shanghai, China) to perform peak integration, calibration, and quantitation for each amino acid.

IMQ-induced Psoriasis-like Mouse Model and Spermidine Treatment

Male BALB/c mice (6–8 weeks of age) were induced by a daily topical dose of IMQ cream (5%) on the shaved back for 6 consecutive days, and then sacrificed for H&E staining. Control mice were treated with the same dose of vehicle cream. Redness, scaling were scored independently on a scale from 0 to 4: 0, none; 1, slight; 2, moderate;

3, marked; 4, very marked. Male BALB/c mice were intraperitoneally injected with spermidine (40mg/kg weight) on day 0, 1, 2 and 3 during the application of IMQ.

Cell Isolation, Flow Cytometry Analysis, and Cell Sorting.

Skin cells were prepared according to previous studies with minor modification (Cai et al., 2011). Briefly, the epidermis and dermis were separated from the skin using dispase (Roche) (25U/ml in 1640), and the epidermal cells was prepared by trypsin (Gibco) digestion, and the dermal cells by collagenase (Sigma-Aldrich) and hyaluronidase (Sigma-Aldrich) digestion. Cells were analyzed using Fortessa (BD) and FlowJo (v10.0.7). Splenocytes were separated by digesting the tissue fragments with collagenase IV (Sigma-Aldrich) and DNase I (Sigma-Aldrich). Antibodies used for cell staining were listed in Table S1. Data were analyzed using Fortessa (BD) and FlowJo (v10.0.7).

Cells were cultured in RPMI 1640 medium (Gibco) with 10% fetal bovine serum (FBS, Gibco) and 1% Penicillin-Streptomycin (Gibco) at 37°C and 5% CO_2 or collected directly for subsequent experiments. To obtain moDCs, mouse monocytes were isolated from BM with the Mouse Monocyte Isolation Kit (BM) according to the technical manual (Miltenyi, Germany). Cells were cultured with 100ng/mL GM-CSF (Peprotech) and 50ng/mL IL-4 (Peprotech) for 7 days and then sorted by Flow cytometry (FACSAriaTM III, BD). IFN-DC were obtained by pre-stimulating moDC with 2000U/mL mouse IFN-α (PBL) for 24 hours. Then, IFN-DC were stimulated with 10μg/mL R837 (Invivogen) for 24 hours. MoDC were stimulated with 1μg/mL LPS (Invivogen) or 5mM ODN2216 (Invivogen) for 24 hours.

ECAR and OCR Measurement

MoDCs were pretreated with or without IFN-α overnight. IFN-DC were incubated with R837 (InvivoGen) in presence or absence of spermidine overnight. Then cells were seeded into XF96-well plates (Agilent) at $2x10^5$ cells per well in 3-6 duplicates. For ECAR test, seahorse base media was supplemented with 2mM glutamine. For the mito-stress OCR test, base media was supplemented with 2mM glutamine (Sigma-Aldrich), 2mM sodium pyruvate (Sigma-Aldrich) and 10mM glucose (Sigma-Aldrich). Plates were incubated in a CO_2 free incubator at 37°C for 1 h and then transfer to the seahorse machine for detection. Measurements were made using an XFe96 Analyzer (Agilent) and results were processed with Wave 2.6.0 software.

Hematoxylin and Eosin Staining

Mouse skin tissues were fixed in formalin and embedded in paraffin. Sections were stained with hematoxylin and eosin. Epidermal hyperplasia was assessed by measuring the thickness of the epidermis from the basal layer to the stratum corneum using Case Viewer software (3DHISTECH Ltd). The epidermal thickness was measured on 10 randomly selected areas per x10 field from three to five fields per skin. All the measurements were performed blinded to the treatment groups. The results were first averaged per mouse and then averaged per treatment group for statistical analysis.

Depletion of Monocytes and Neutrophils

The depletion was performed as previously described. Briefly, to deplete monocytes and neutrophils, the mice were injected intraperitoneally with 500mg/mice/day of anti-Gr1 (clone RB6-8C5, BioXCell, West Lebanon, NH, USA) on days 0, 1, 2, 3 and 4. To deplete neutrophils alone, the mice were injected intraperitoneally with 500mg/mice/day anti-Ly6G (clone 1A8, BioXCell, West Lebanon, NH, USA) using the same schedule.

MRNA-sequencing

Total RNA was extracted by Trizol reagent (Invitrogen) and determined by Bioanalyzer 4200 (Agilent, Santa Clara, CA, USA). Then, the next-generation libraries of mRNA were prepared using VAHTS mRNA-seq v2 Library Prep Kit for Illumina® (Vazyme, Nanjing, China). The Library quality was determined by Bioanalyzer 4200 (Agilent, Santa Clara, CA, USA). Then the mRNA-seq libraries were sequenced in HiSeq x10 system (Illumina, San Diego, CA, USA) on a 150bp paired-end run. The differentially expressed genes were selected as having more than 1 fold difference in their geometrical mean expression between the compared groups and a statistically significant p-value (<0.05) by analysis of DEseq2. The GO analysis on differentially expressed genes was performed with an R package: Clusterprofiler using a $p<0.05$ to define statistically enriched GO categories. Pathway analysis was used to determine the significant pathway of the differential genes according to Kyoto Encyclopedia of Genes and Genomes Database (http://www.genome.jp/kegg/) and DAVID Bioinformatics Resources 6.8 (https://david.ncifcrf.gov/).

Quantitative Real-time RT–PCR

Total RNA of moDCs and IFN-DCs was extracted by Trizol reagent (Invitrogen). The extraction of RNA from whole skins were performed using RNeasy Fibrous Tissue Mini Kit (Qiagen, Hilden, Germany) according to the manufacturer's instructions. cDNA was prepared by reverse transcription (PrimeScript RT Reagent kit; Takara) and amplified by real-time quantitative PCR (qPCR) with the primers shown in Table S2. Amplification was performed in an ABI PRISM 7900 Real Time PCR System (Applied Biosystems). The amplification efficiency of these genes was the same as that for *β-actin*, as indicated by the standard curves for amplification. The expression of mRNAs were normalized to *β-actin* mRNA by calculating $2^{-\Delta Ct}$, where Ct is the cycle threshold.

Immunoblots

2×10^6 DCs were lysed in radioimmune precipitation assay lysis and extraction buffer (Thermo Fisher Scientific). Nuclear and cytoplasmic extracts were prepared using a NE-PER Nuclear and Cytoplasmic Extraction Kit (Thermo Fisher Scientific). Individual cell lysates (10μg/lane) were separated by 10% SDS-PAGE and transferred to an Immobilon-P polyvinylidene difluoride membrane (Millipore, Billerica, MA). After being blocked with SuperBlock T20 PBS blocking buffer (Thermo Fisher Scientific, Pittsburgh, PA), the membranes were incubated with antibodies listed in the

Table S1.

Cytokine Detection

Serum from IMQ induced mice were collected on indicated time points, and cytokines were detected by BD™ Cytometric Bead Array (CBA) Mouse Flex Sets. Mouse serum IFN-α was detected by Mouse IFN α ELISA Kit (PBL, 42120-1). Cell supernatant was collected and analyzed by ELISA kit according to manufacturer's instructions for IL-6 (Biolegend, 431307), TNF-α (Biolegend, 430907), and IL-12/IL-23 p40 (Thermo Fisher, 88-7120-22).

Statistics

For all experiments, data were analyzed by two-tailed unpaired *t* test or one-way ANOVA. The data were analyzed by Graph Prism 7.0 software (GraphPad Software Inc.), p values were provided as * $p < 0.05$, ** $p < 0.01$, *** $p < 0.001$, n.s. not significant.

Data and Software Availability

RNA seqencing transcriptomic data are deposited in the Gene Expression Omnibus repository (GSE142452).

References

Cai, Y., Shen, X., Ding, C., Qi, C., Li, K., Li, X., Jala, V.R., Zhang, H.G., Wang, T., Zheng, J., et al. (2011). Pivotal role of dermal IL-17-producing gammadelta T cells in skin inflammation. Immunity 35, 596-610.

Chen, T., Ni, Y., Ma, X., Bao, Y., Liu, J., Huang, F., Hu, C., Xie, G., Zhao, A., Jia, W., et al. (2016a). Branched-chain and aromatic amino acid profiles and diabetes risk in Chinese populations. Sci Rep 6, 20594.

Chen, T., Zheng, X., Ma, X., Bao, Y., Ni, Y., Hu, C., Rajani, C., Huang, F., Zhao, A., Jia, W., et al. (2016b). Tryptophan Predicts the Risk for Future Type 2 Diabetes. PLoS One 11, e0162192.

Supplemental Figure legends

Figure S1. Sorting strategy of moDCs, Related to Figure 1. (A) MoDCs were sorted as $FV575^{-}CD11c^{+}MHCII^{hi}CD11b^{int}$ cells. FV575, live/die dye. FSC-A, FSC-W, SSC-A and SSC-W were used to gate single cells. (B, left) The expression of F4/80 in moDCs and macrophage. (B, right) The morphology of sorted moDCs and macrophages. (C) The purity of sorted moDCs. All the data are representative of three independent experiments.

Figure S2. Spermidine do not affect the apoptosis of IFN-DCs, Related to Figure 2. (A) BM monocytes were cultured with GM-CSF and IL-4 for 7 days. MoDCs were sorted and treated with 2000U/mL IFN-α for 24 hours. Then, IFN-DCs were stimulated with R837, together with or without 15μM spermidine for 24 hours. The survival of IFN-DC was detected by using flow cytometry. Live cells, $FV575^{-}$ cells. Data are representative of three independent experiments. (B) Sorted moDCs were stimulated with IFN-α alone or IFN-α plus SPD overnight. The relative mRNA levels of *TLR7* are shown (n=3). (C) TLR7 transfected moDCs were pretreated with or without 1 mM DFMO, and then stimulated with R837 for 24 hours. The expression of TNF-α and IL-6 are shown (n=3). (D) MoDCs were primed with IFN-α or IFN-α plus SPD, and then stimulated with R837 for 24 hours. The expression of TNF-α and IL-6 are shown (n=3). (E) MoDCs were stimulated with 1μg/mL LPS or 5μM ODN2216 together with or without 30μM SPD for 24 hours. The protein levels of TNF-α and IL-6 are shown (n=3). All data are representative of two independent experiments and shown as mean ±SEM. p values were determined by two-tailed unpaired t test *p<0.05, **p<0.01, ***p<0.001.

Figure S3. Spermidine inhibits autoimmune related pathways, Related to Figure 4. IFN-DCs were cultured with R837, together with or without spermidine for 18 hours. Cells were collected and the mRNA expression was detected by RNA-seq. Changed genes enriched pathways were shown.

Figure S4. FOXO3 partially mediates the anti-inflammatory effect of Spermidine, Related to Figure 4. (A) The ratios of phosphorylated protein to total protein at 0min time point were set as 1, respectively. (B) The ratios of phosphorylated protein to total protein at 0min time point of SPD group were set as 1, respectively. Data are representative of three independent experiments and shown as mean ±SEM. p values were determined by two-tailed unpaired *t* test *p<0.05, **p<0.01, ***p<0.001. The difference at 30min time point in (B) were statistically analyzed. (C) BM cells were isolated from WT or *Foxo3a*$^{-/-}$ mice, and the expression of FOXO3 was detected by immunoblot. Data are representative of two independent experiments.

Figure S5. IMQ induces the expression of IFN-α and TLR7 while spermidine hampers the induction, Related to Figure 5. (A) Mice were painted with IMQ on the back and ear. 8 hours later, the expression of IFN-α in serum were detected. (B) The expression of *TLR7* mRNA in the dermal moDCs isolated from IMQ induced mice at

indicated time points. (C) The expression of *TLR7* mRNA in the dermal moDCs isolated from IMQ induced mice with or without spermidine treatment on day 4. The expression of mRNAs were normalized to *β-actin* mRNA by calculating $2^{-\Delta Ct}$ (n=5). Data are representative of two independent experiments and shown as mean ±SEM. p values were determined by two-tailed unpaired *t* test. *p<0.05, **p<0.01, ***p<0.001, n.s. not significant.

Figure S6. Administration of spermidine ameliorates the systematic inflammation of IMQ-induced psoriasis-like mice, Related to Figure 5. Mice were treated with IMQ and spermidine as the schedule shown in Figure 5A. (A) Pictures and weight of spleen (n=5-7). (B) Gating strategy of splenocytes. (C) The number of splenic $Ly6c^{hi}$ monocytes, macrophages, neutrophils, B cells, pDCs, $CD8\alpha^+$ cDCs, $CD8\alpha^-$ cDCs, $CD4^+$ T cells and $CD8^+$ T cells (n=5). Data are representative of two independent experiments and shown as mean ±SEM. p values compare the indicated groups using a two-tailed unpaired Student's *t* test. *p<0.05, **p<0.01, n.s. not significant.

Figure S7. Spermidine inhibits the infiltration of moDCs and activation of γδT cells, Related to Figure 5. (A) Flow cytometry analysis of moDC or (B) $IL\text{-}17A^+$ γδT in the dermal skin from IMQ induced mice with or without spermidine treatment.

Figure S8. IFN-DC participates in the anti-psoriasis process of spermidine, Related to Figure 6. (A) The depletion efficiency of anti-Gr1 and anti-Ly6G antibody in vivo. (B) The number of macrophages, neutrophils, B cells, pDCs, $CD8\alpha^+$ cDCs, $CD8\alpha^-$ cDCs, $CD4^+$ T cells and $CD8^+$ T cells from the spleen of indicated mice in Figure 6 (n=5). Data are representative of two independent experiments and shown as mean ±SEM. p values were determined by two-tailed unpaired *t* test. *p<0.05, **p<0.01, ***p<0.001, n.s. not significant.

Supplemental Tables

Table S1. Antibody list used in the paper, Related to Figure 2-6.
Table S2. Primer list used in the paper, Related to Figure 1 and 5.

Figure S1

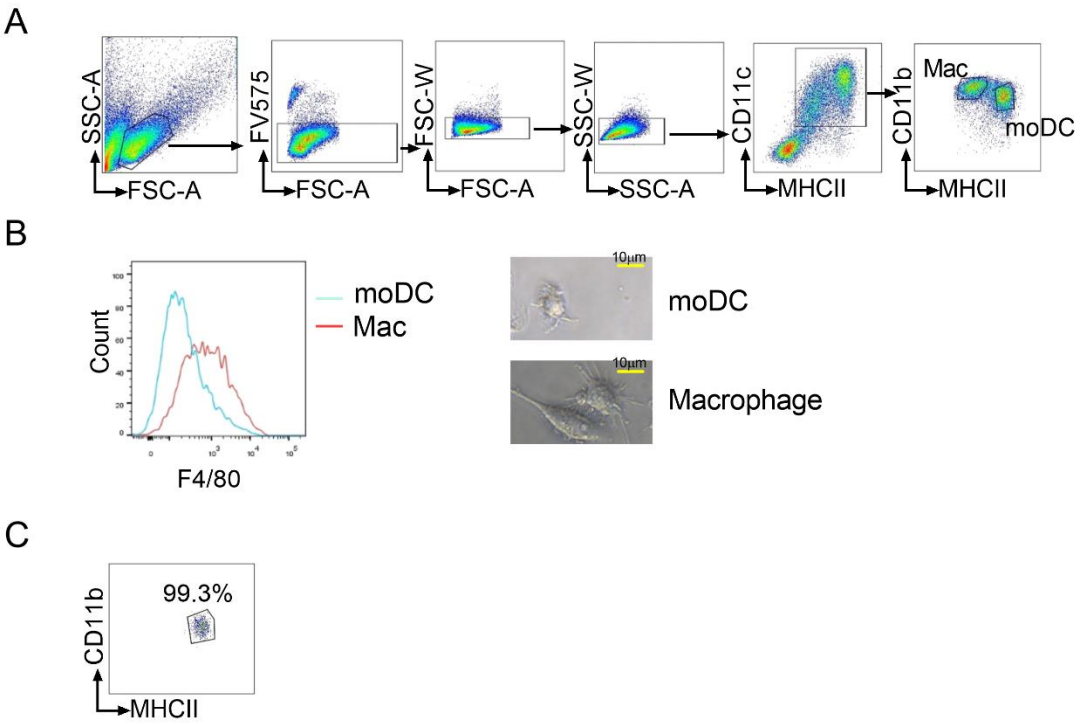
A
SSC-A
FSC-A
FV575
FSC-A
FSC-W
FSC-A
SSC-W
SSC-A
CD11c
MHCII
CD11b
MHCII
Mac
moDC
B
Count
F4/80
moDC
Mac
10μm
moDC
10μm
Macrophage
C
CD11b
MHCII
99.3%

Figure S2

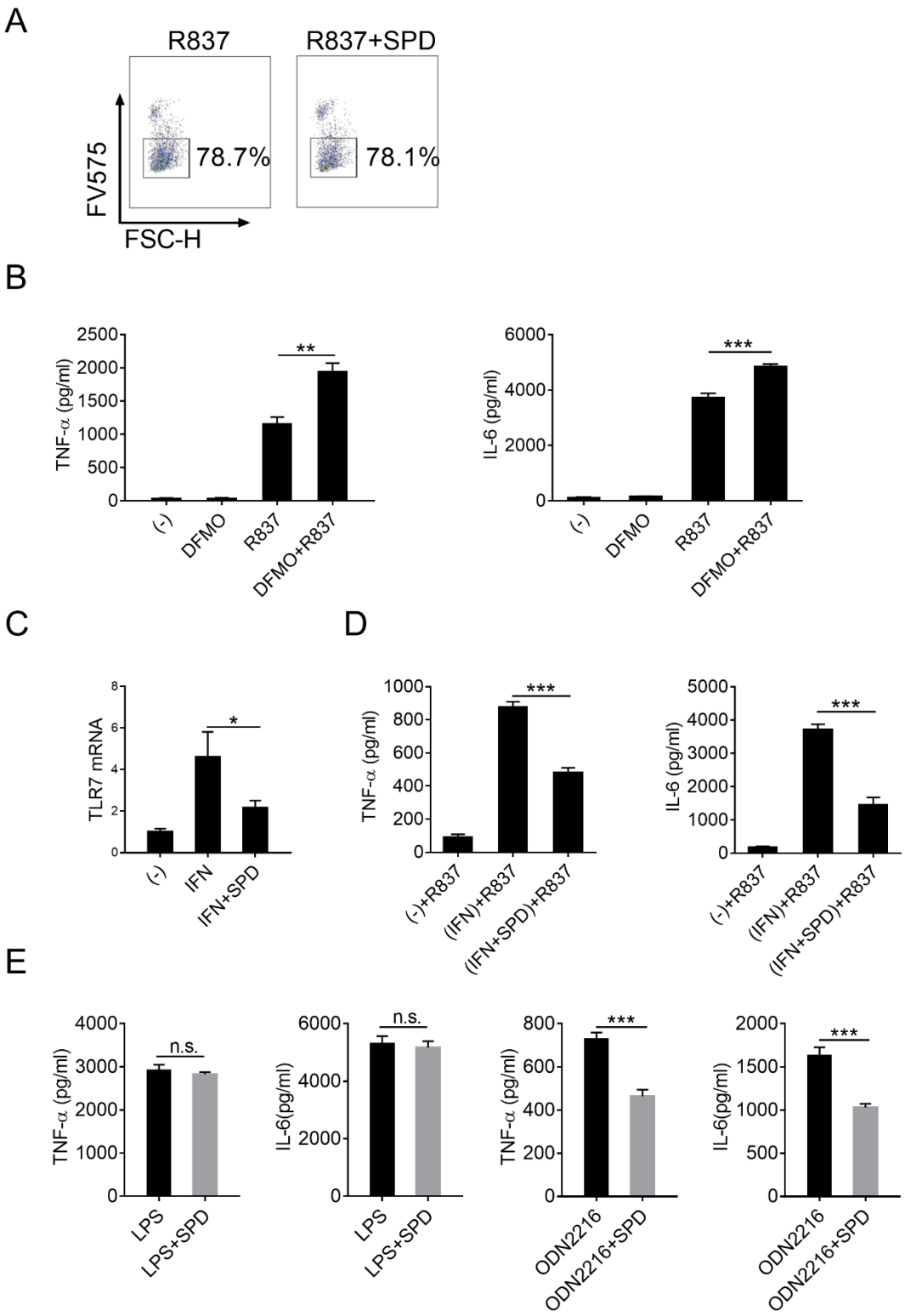
A
R837
R837+SPD
78.7%
78.1%
FV575
FSC-H
B
TNF-α (pg/ml)
IL-6 (pg/ml)
(-)
DFMO
R837
DFMO+R837
C
TLR7 mRNA
IFN
IFN+SPD
D
(-)+R837
(IFN)+R837
(IFN+SPD)+R837
E
n.s.
LPS
LPS+SPD
IL-6(pg/ml)
ODN2216
ODN2216+SPD

Figure S3

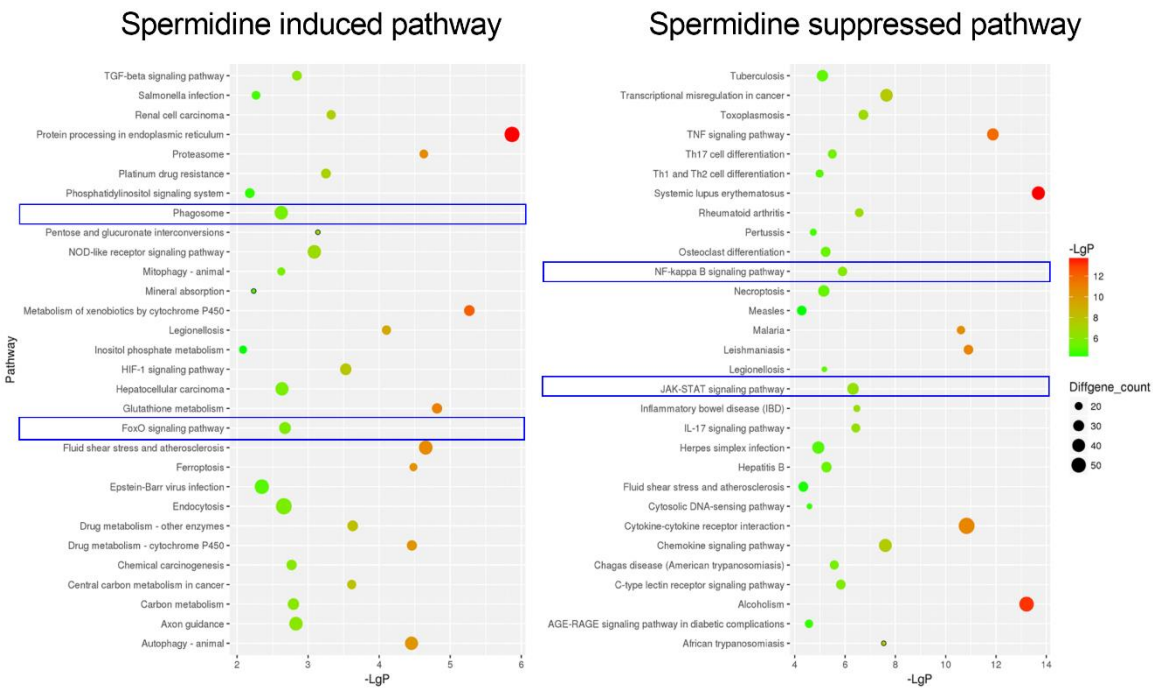
Spermidine induced pathway
Spermidine suppressed pathway
TGF-beta signaling pathway
Salmonella infection
Renal cell carcinoma
Protein processing in endoplasmic reticulum
Proteasome
Platinum drug resistance
Phosphatidylinositol signaling system
Phagosome
Pentose and glucuronate interconversions
NOD-like receptor signaling pathway
Mitophagy - animal
Mineral absorption
Metabolism of xenobiotics by cytochrome P450
Legionellosis
Inositol phosphate metabolism
HIF-1 signaling pathway
Hepatocellular carcinoma
Glutathione metabolism
FoxO signaling pathway
Fluid shear stress and atherosclerosis
Ferroptosis
Epstein-Barr virus infection
Endocytosis
Drug metabolism - other enzymes
Drug metabolism - cytochrome P450
Chemical carcinogenesis
Central carbon metabolism in cancer
Carbon metabolism
Axon guidance
Autophagy - animal
Pathway
2
3
4
5
6
-LgP
Tuberculosis
Transcriptional misregulation in cancer
Toxoplasmosis
TNF signaling pathway
Th17 cell differentiation
Th1 and Th2 cell differentiation
Systemic lupus erythematosus
Rheumatoid arthritis
Pertussis
Osteoclast differentiation
NF-kappa B signaling pathway
Necroptosis
Measles
Malaria
Leishmaniasis
Legionellosis
JAK-STAT signaling pathway
Inflammatory bowel disease (IBD)
IL-17 signaling pathway
Herpes simplex infection
Hepatitis B
Fluid shear stress and atherosclerosis
Cytosolic DNA-sensing pathway
Cytokine-cytokine receptor interaction
Chemokine signaling pathway
Chagas disease (American trypanosomiasis)
C-type lectin receptor signaling pathway
Alcoholism
AGE-RAGE signaling pathway in diabetic complications
African trypanosomiasis
4
6
8
10
12
14
-LgP
-LgP
12
10
8
6
Diffgene_count
20
30
40
50

Figure S4

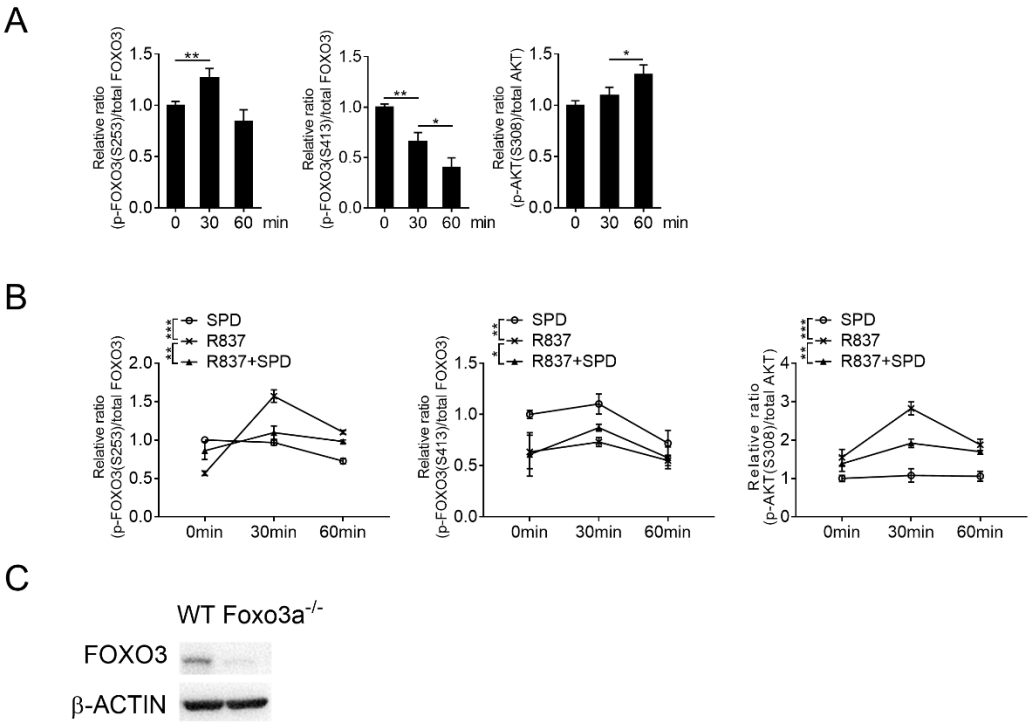
A
Relative ratio (p-FOXO3(S253)/total FOXO3)
Relative ratio (p-FOXO3(S413)/total FOXO3)
Relative ratio (p-AKT(S308)/total AKT)
0 30 60 min
B
SPD
R837
R837+SPD
Relative ratio (p-FOXO3(S253)/total FOXO3)
Relative ratio (p-FOXO3(S413)/total FOXO3)
Relative ratio (p-AKT(S308)/total AKT)
0min 30min 60min
C
WT Foxo3a-/-
FOXO3
β-ACTIN

Figure S5

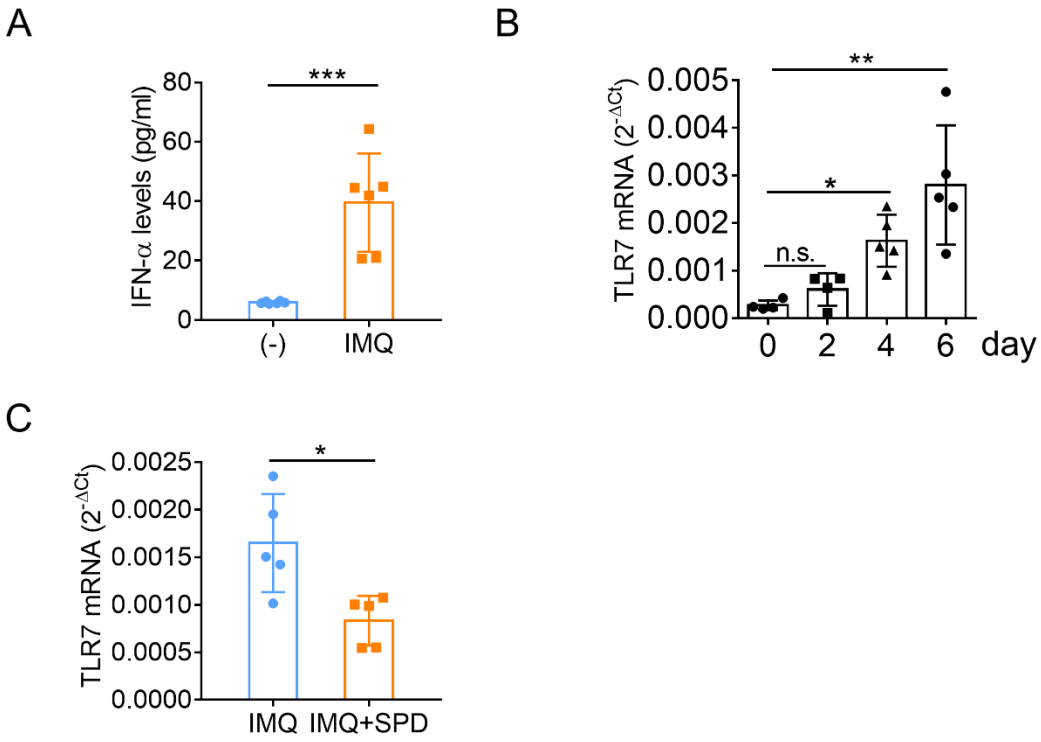
A
IFN-α levels (pg/ml)
80
60
40
20
0
***
(-)
IMQ
B
TLR7 mRNA (2^-ΔCt)
0.005
0.004
0.003
0.002
0.001
0.000
**
*
n.s.
0
2
4
6
day
C
TLR7 mRNA (2^-ΔCt)
0.0025
0.0020
0.0015
0.0010
0.0005
0.0000
*
IMQ
IMQ+SPD

Figure S6

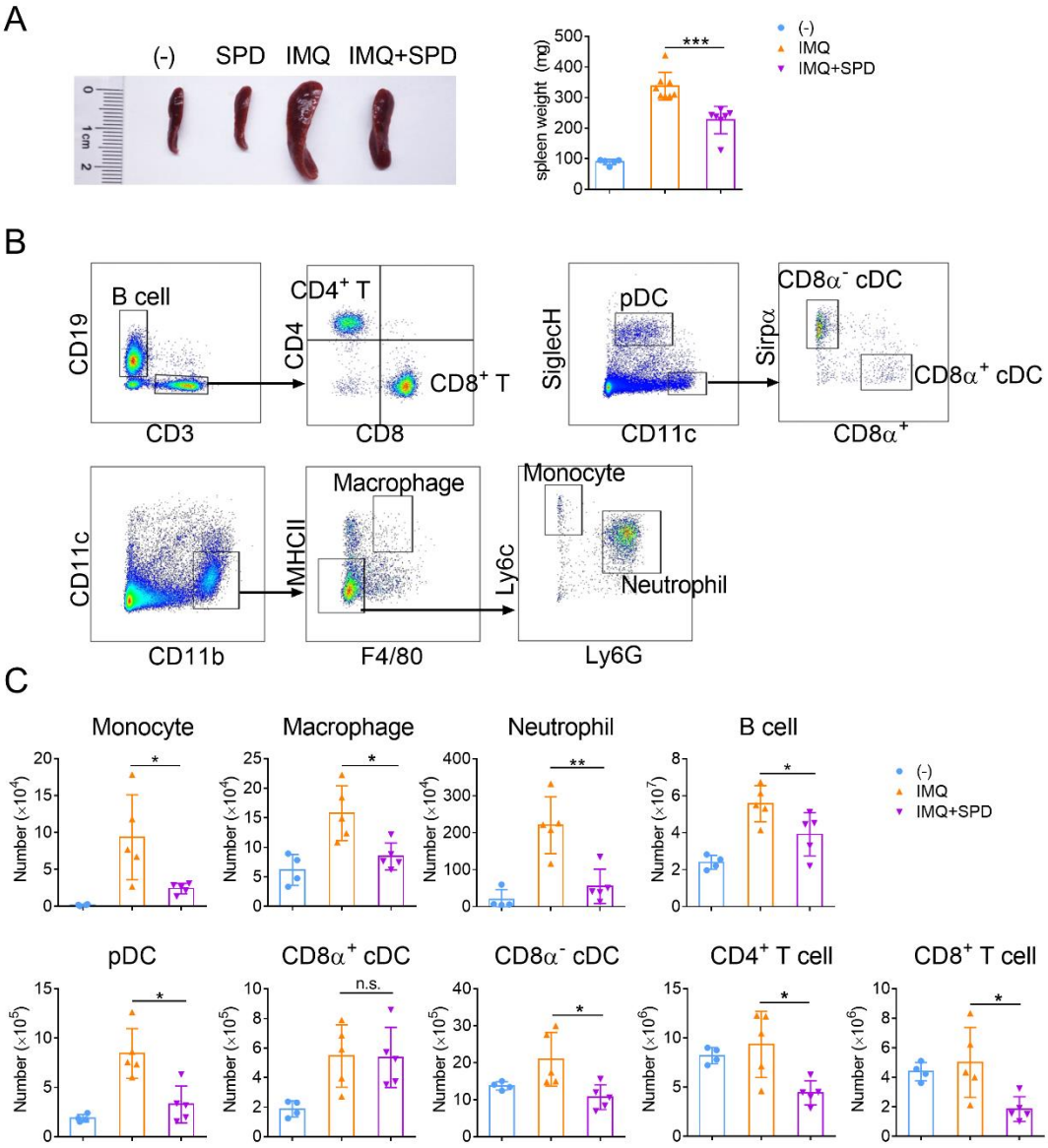
A
(-)
SPD
IMQ
IMQ+SPD
spleen weight (mg)
***
B
B cell
CD19
CD3
CD4⁺ T
CD4
CD8⁺ T
CD8
pDC
SiglecH
CD11c
CD8α⁻ cDC
Sirpα
CD8α⁺ cDC
CD8α⁺
CD11c
CD11b
Macrophage
MHCII
F4/80
Monocyte
Ly6c
Neutrophil
Ly6G
C
Monocyte
Macrophage
Neutrophil
B cell
pDC
CD8α⁺ cDC
CD8α⁻ cDC
CD4⁺ T cell
CD8⁺ T cell
Number (×10⁴)
Number (×10⁷)
Number (×10⁵)
Number (×10⁶)
n.s.
(-)
IMQ
IMQ+SPD

Figure S7

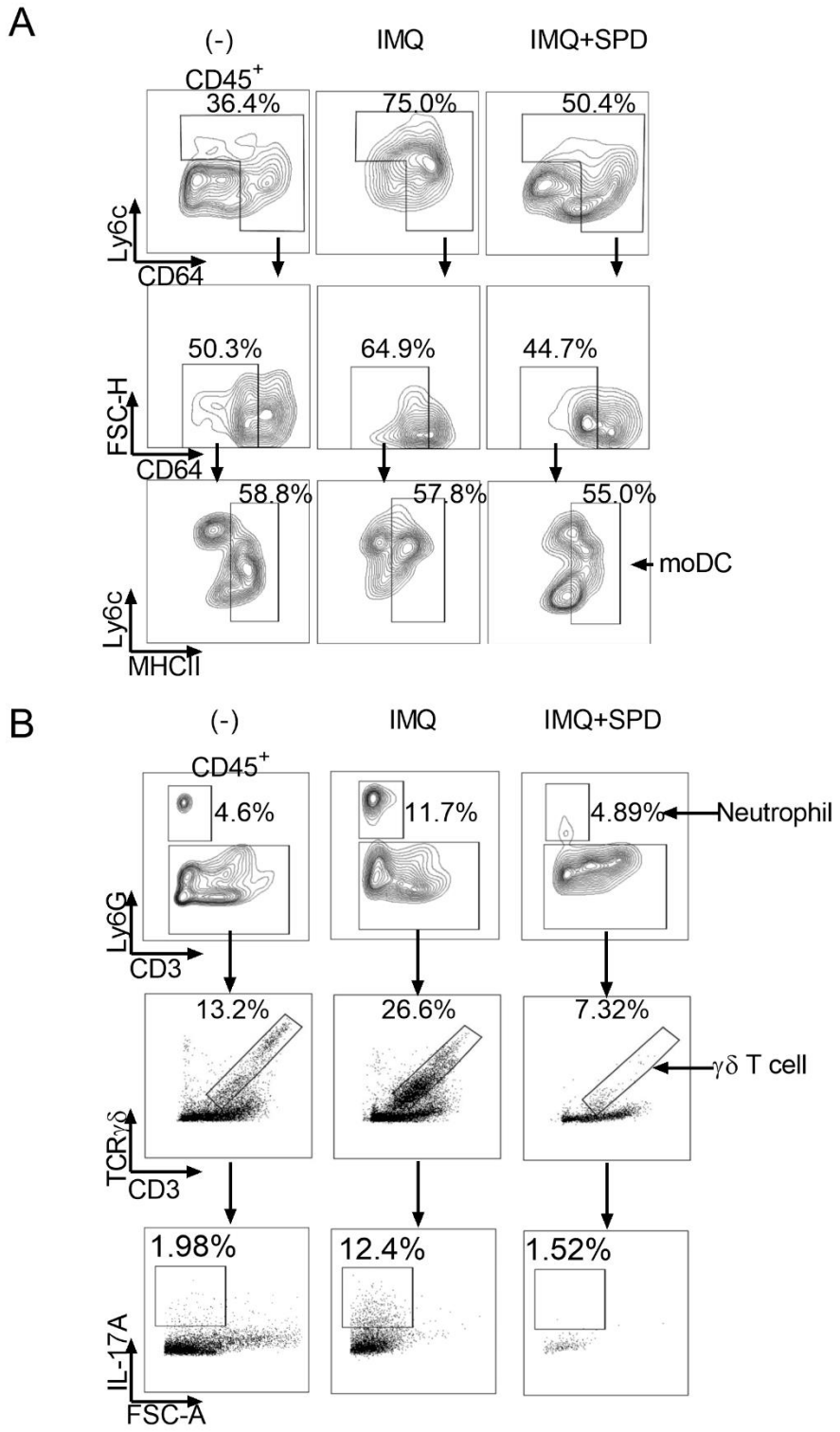
A
(-)
IMQ
IMQ+SPD
CD45+
36.4%
75.0%
50.4%
Ly6c
CD64
50.3%
64.9%
44.7%
FSC-H
CD64
58.8%
57.8%
55.0%
moDC
Ly6c
MHCII
B
(-)
IMQ
IMQ+SPD
CD45+
4.6%
11.7%
4.89%
Neutrophil
Ly6G
CD3
13.2%
26.6%
7.32%
γδ T cell
TCRγδ
CD3
1.98%
12.4%
1.52%
IL-17A
FSC-A

Figure S8

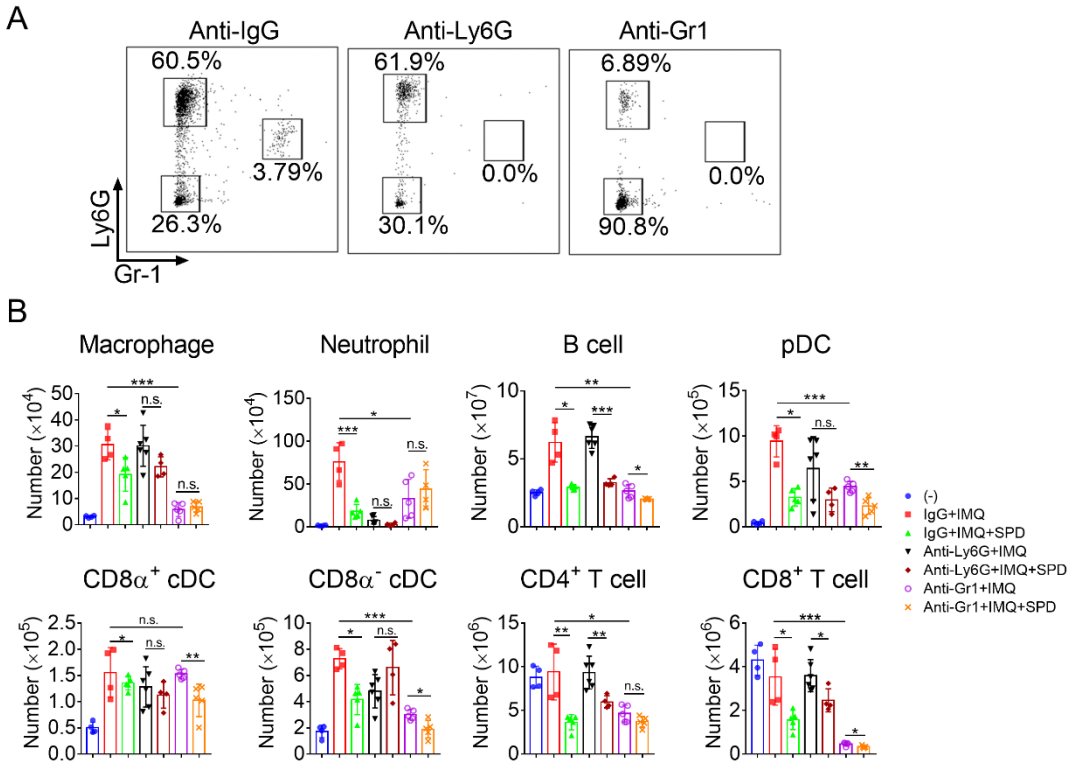
A
Anti-IgG
Anti-Ly6G
Anti-Gr1
60.5%
3.79%
26.3%
61.9%
0.0%
30.1%
6.89%
0.0%
90.8%
Ly6G
Gr-1
B
Macrophage
Neutrophil
B cell
pDC
CD8α+ cDC
CD8α- cDC
CD4+ T cell
CD8+ T cell
Number (×10^4)
Number (×10^7)
Number (×10^5)
Number (×10^6)
n.s.
(-)
IgG+IMQ
IgG+IMQ+SPD
Anti-Ly6G+IMQ
Anti-Ly6G+IMQ+SPD
Anti-Gr1+IMQ
Anti-Gr1+IMQ+SPD

Table S1

Antibodies	Source	Cat#
Anti-mouse CD45 - APC-CY7	BioLegend	103116
Anti-mouse CD3 - PE-CY7	BioLegend	100220
Anti-mouse CD4 - FITC	BioLegend	100406
Anti-mouse TCR γδ - APC	BioLegend	118116
Anti-mouse Ly6G - Percp-cy5.5	BioLegend	127616
Anti-mouse MHC Ⅱ - BV510	BioLegend	107636
Anti-mouse CD64 - PE	BioLegend	139304
Anti-mouse Ly6C - FITC	BioLegend	128006
Anti-mouse CD11b - PE-CY7	BioLegend	101216
Anti-mouse CD11c - Percp-cy5.5	BioLegend	117328
Anti-mouse CD103 - FITC	BioLegend	121420
Anti-mouse CD19 - BV510	BioLegend	115546
Anti-mouse CD11c - FITC	BioLegend	117306
Anti-mouse Ly6C - BV605	BioLegend	128036
Anti-mouse CD8α - PE-CY7	BioLegend	100722
Anti-mouse CD8α - Percp-cy5.5	BioLegend	100733
Anti-mouse IL17A - PE	BD	559502
Anti-mouse Siglec H – PE-CY7	Invitrogen	25-0333-82
Anti-mouse CD45 - APC	BioLegend	103112
Anti-mouse CD107a - APC	BioLegend	144014
Anti-mouse Ly6G - APC	BioLegend	127614
Anti-mouse CD3 - APC	BioLegend	100236
Anti-mouse Ly6G/Ly6C(Gr-1) - APC	BioLegend	108412
Anti-mouse CD40 - PE-CY7	BioLegend	124622
Anti-mouse CD86 - Percp-cy5.5	BioLegend	105028
Anti-mouse I-A/I-E- BV510	BioLegend	107641
NF-κB P65(D14E12)	CST	8242
Phospho-NF-κB P65 (Ser536) Antibody	CST	3033
β-Actin(13E5) Rabbit mAb	CST	4970
AMPKα (D5A2) Rabbit mAb	CST	5831
Phospho-AMPKα (Thr172) (40H9) Rabbit mAb	CST	2535
Phospho-4E-BP1 (Thr37/46) (236B4) Rabbit mAb	CST	2855
4E-BP1 (53H11) Rabbit mAb	CST	9644
Phospho-p70 S6 Kinase (Thr389) antibody	CST	9205
p70 S6 Kinase antibody	CST	9202
Phospho-Raptor (Ser792) antibody	CST	2083
Raptor (24C12) Rabbit mAb	CST	2280
Phospho-Akt (Ser473) Antibody	CST	9271
Akt antibody	CST	9272
Phospho-FoxO3a (Ser253) Antibody	CST	9466

Phospho-FoxO3a (Ser413) (D77C9) Rabbit mAb	CST	8174
FoxO3a (D19A7) Rabbit mAb	CST	12829
Anti-mouse IgG, HRP-linked antibody	CST	7076
Anti-rabbit IgG, HRP-linked antibody	CST	7074
Anti-mouse Ly6G	BioCell	1A8
Anti-mouse Ly6G/Gr1	BioCell	RB6-8C5
Lamin B1 Antibody	proteintech	66095-1-Ig

Table S2

species	gene	Forward(5'-3')	Reverse(5'-3')
mouse	*Arg1*	CATTGGCTTGCGAGACGTAGAC	GCTGAAGGTCTCTTCCATCACC
	Odc1	TGCCACACTCAAAACCAGCAGG	ACACTGCCTGAACGAAGGTCTC
	β-actin	GGCTGTATTCCCCTCCATCG	CCAGTTGGTAACAATGCCATGT
	Sms	GATGTACGCCAAAGAAGGGAGAG	CAGGTCGAGAATCAGTCTGAGG
	Srm	CGTTGGCTTCTCCAGCTCAAAG	AGGACTCCTTGAAGAGGCTCTC
	Ssat1	GAGGATGGCTTTGGAGAACACC	GATACAGCAACTTGCCAATCCATG
	Nos2	GAGACAGGGAAGTCTGAAGCAC	CCAGCAGTAGTTGCTCCTCTTC
	IL-17a	GAC TCT CCA CCG CAATGA	CTT CAG GAC CAG GAT CTC TT
	IL-23a	CAA CTC CTC CAG CCA GAG	GAA CCT GGG CAT CCT TAA
	IL-6	TGA AGT TCC TCT CTG CAA GA	GAA GTG GTA TAG ACA GGT CTG TT
	TNF-α	TCG GGT TGA GAA GAT CAT T	TAG ATT CCT GGA AGC ATA GAA